NASA-CR-72420

OXIDATION BEHAVIOR OF CO-25CR AND CO-35CR ALLOYS

by

P. Kofstad and A. Z. Hed
Metal Science Group

prepared for

NATIONAL AERONAUTICS AND SPACE ADMINISTRATION

under

RESEARCH GRANT NGR-36-002-070

on

HIGH-TEMPERATURE OXIDATION OF ALLOYS:
COBALT-CHROMIUM BASE ALLOYS

June 4, 1968

BATTELLE MEMORIAL INSTITUTE
Columbus Laboratories
505 King Avenue
Columbus, Ohio 43201

NASA-CR-72420

TOPICAL REPORT

Covering the Period
November 1, 1967-March 31, 1968

OXIDATION BEHAVIOR OF Co-25Cr AND Co-35Cr ALLOYS

by

Per Kofstad and A. Z. Hed
Metal Science Group

prepared for

NATIONAL AERONAUTICS AND SPACE ADMINISTRATION

June 4, 1968

under
RESEARCH GRANT NGR-36-002-070
on
High-Temperature Oxidation of Alloys:
Cobalt-Chromium Base Alloys

Technical Management
NASA Lewis Research Center
Cleveland, Ohio
Materials and Structures Division
James S. Wolf
Frederic H. Harf

BATTELLE MEMORIAL INSTITUTE
Columbus Laboratories
505 King Avenue
Columbus, Ohio 43201

ABSTRACT

The oxidation of Co-25Cr and Co-35Cr may be characterized as follows:

At high oxygen partial pressure, the total cross-sectional area of the CoO channels in the scale formed on Co-25Cr alloys exceeds 0.1 percent of the total diffusional area. The rate-controlling process is diffusion of Co in these CoO channels.

At low oxygen pressure during the oxidation of Co-25Cr, the total cross-sectional area of these channels decreases below the 0.1 percent level, and the channels are probably blocked completely. The rate-controlling process is the solid-state diffusion of Cr cations in a predominantly $CoCr_2O_4$ scale.

The initial oxidation behavior may be explained on the basis of the transformation to spinel of the Cr_2O_3 layer produced preferentially during the preoxidation stages and perhaps also during the first stages of oxidation.

TABLE OF CONTENTS

LIST OF TABLES

LIST OF FIGURES

LIST OF FIGURES
(Continued)

LIST OF FIGURES
(Continued)

OXIDATION BEHAVIOR OF Co-25Cr AND Co-35Cr ALLOYS

by

Per Kofstad* and A. Z. Hed

INTRODUCTION

The purpose of the work reported herein was to study the high-temperature oxidation behavior of Co-25Cr and Co-35Cr and devise a comprehensive theory to explain that observed behavior.

Cobalt-chromium alloys serve as the basis materials for a family of cobalt-base superalloys for high-temperature applications. In efforts to increase the use temperatures of such alloys, the question of chemical stability and, particularly, oxidation resistance becomes of paramount importance. The development of oxidation-resistant alloys has to a large extent been empirical in nature, therefore, a detailed understanding of mechanisms of high-temperature oxidation of alloys is lacking.

During the second semiannual period of Research Grant NGR-36-002-070, the research has covered studies on the oxidation of Co-Cr alloys containing 1.5, 10, 25, and 35 percent chromium. Prelimimary results on the creep behavior of CoO single crystals and on the defect structure of CoO and Cr-doped CoO have been obtained and will be reported under a separate cover.

A literature survey pertaining to the material involved in the present study was reported in the first semiannual report on high-temperature oxidation of Co-Cr base alloys and will not be included.

SUMMARY

The present topical report covers the results of the oxidation behavior of the chromium-rich Co-Cr alloys, Co-25Cr and Co-35Cr. The oxidation behavior of these alloys is complex and does not follow a single mechanism. For the Co-25Cr alloy, the parabolic rate constants at high oxygen pressures (p_{O_2} > 100 torr) in the temperature range of 900 to 1300 C are about two orders of magnitude larger than at low oxygen pressures (p_{O_2} < 10 torr). The oxidation rate of Co-35Cr is almost independent of oxygen pressure over the range 0.2 to 760 torr O_2 and is comparable to the low-oxygen-pressure oxidation rate of Co-25Cr alloys.

The scale formed on Co-25Cr oxidized at high oxygen pressure consists of two layers, an outer layer of CoO and an inner layer of $CoCr_2O_4$ and small amounts of CoO. The scale formed on Co-35Cr at all pressures and on Co-25Cr at low pressure is single layered and consists mainly of $CoCr_2O_4$, with some Cr_2O_3. The relative distributions have not as yet been established.

It is believed that the oxidation mechanism of Co-25Cr involves cobalt-cation diffusion through a CoO network in the inner layer. During the initial stage of oxidation,

*Present address: Central Institute for Industrial Research, Oslo-Blindern, Norway.

the effective diffusional area is constantly changing, resulting in a nonparabolic behavior, until this area reaches stabilization. Then oxidation proceeds according to a parabolic law. The stabilized effective diffusional area decreases with decreasing oxygen partial pressure, by the growth of spinel, until complete blocking results. Then the oxidation proceeds by the diffusion of both Co and Cr through the spinel. At low pressures the spinel blocking is achieved, and the parabolic rate constant decreases by two orders of magnitude. In this case, the oxidation rate is determined by the slowest-moving species in the spinel, probably Cr^{3+}, and is increased to some degree by a short-circuiting effect of the pores in the scales. It is believed that, during the initial stage of oxidation, preferential oxidation of chromium occurs; however, the extent of this feature has not yet been determined.

MATERIALS AND METHODS

Alloys with the nominal composition Co-25Cr and Co-35Cr were prepared in a vacuum furnace and cast in a tapered zirconite sand mold. The dimensions of the mold were: top, 6.3 x 6.3 cm; bottom, 3.0 x 3.8 cm; length, 24.5 cm. Subsequent chemical analysis showed that the alloy compositions were Co-24.6Cr and Co-34.3Cr.

After sandblasting, the ingots were heat treated at 1125 C for 2 hours and then forged at high temperatures to the size 2.2 x 6.3 x 43.1 cm. The optimum forging temperatures for these alloys appeared to be 1150 to 1200 C for Co-25Cr and 1200 to 1250 C for Co-35Cr.

The forged plates were then hot rolled to a 0.22-cm thickness and subsequently cold rolled to a thickness of about 0.18 cm. After rolling, the sheets were again sandblasted. The sheets were then cut into specimens measuring 2.5 x 1.9 cm; these specimens were subsequently ground on emery paper and diamond polished. The polishing procedure removed some 50 to 100 microns of material. The final thickness of the specimens varied between 0.15 and 0.165 cm. The specimens were then measured and washed in water and trichloroethylene. A metallographic inspection of these specimens revealed Cr_2O_3 inclusions in the alloy; these are probably due to oxygen contamination during casting, forging, and hot rolling.

The high-temperature oxidation of Co-25Cr and Co-35Cr was studied by continuously measuring the weight change of specimens exposed to oxidizing environments at the different temperatures. Specimens were oxidized in air in an open furnace with a Crusilite heating element. A Mullite tube served as a reacting chamber. The temperature was measured with a Pt/Pt-10 Rh thermocouple and controlled by an on-off Barber-Coleman controller to within 3 C. The weight change was continuously recorded with an Ainsworth automatic recording balance. Weight change could be determined to within 0.3 mg, or 0.03 mg/cm^2.

Oxidation rates in controlled oxygen atmospheres were measured with an automatic Cahn Rh electrobalance enclosed in a high-vacuum system. The balance was used with a sensitivity of 100 μg, and the weight gain was continuously recorded on an AZAR Leeds and Northrup recorder. Temperature in the Mullite-tube reaction chamber was controlled and measured as described above. The system was pumped down with a 450-liter CVC diffusion pump and an Edwards mechanical pump. Pressures down to 10^{-5} torr were achieved, as measured on the CVC ionization and thermocouple gage.

The specimens were connected to the balance with Pt-10 Rh wire and placed in a cold side-tube of the apparatus, and then the system was evacuated. After the furnace was temperature equilibrated and, while still under the high vacuum (10^{-4} to 10^{-5} torr), specimens were lowered into the hot zone by a magnetic device. Oxygen was then admitted to the system through a Granville-Phillips metering needle valve. One to two minutes generally elapsed from the time the specimens were loaded into the hot zone until the desired oxygen pressure in the system was reached. Zero time for the oxidation was taken as the instant when the desired oxygen pressure was attained. At the lower oxygen pressures ($\leq$10 torr), oxygen was continuously pumped through the system during the oxidation.

After the specimens had been oxidized to the desired extent, they were raised out of the hot zone. The system was backfilled with oxygen, and the specimens were taken out and quenched in a molten lead-bismuth alloy, which in turn was rapidly cooled and solidified. In this manner, spallation of the oxide scales was prevented.

A limited number of oxidized specimens were chosen for further examination and characterization by means of metallographic techniques and X-ray diffraction.

RESULTS OF THERMOGRAVIMETRIC STUDIES

The rate of oxidation of diamond-polished Co-25Cr and Co-35Cr alloys was studied in the temperature range 900-1300 C. The oxidation was carried out either in air or in pure oxygen in the pressure range 0.2 to 760 torr.

In Figures 1 through 3, the weight gain of the Co-25Cr alloy during oxidation is plotted versus time in different oxygen partial pressures at temperatures of 1000, 1100, and 1300 C, respectively. In Figures 4 to 7, the square of the weight gain during oxidation of Co-25Cr alloy is plotted versus time in different oxygen partial pressures in the temperature range 900-1300 C.

The linear plots in Figures 4-7 reveal a typical behavior at high oxygen partial pressures. These lines can be divided into two parts, an initial undefined oxidation rate and a typical parabolic rate at later stages. At lower oxygen pressures, typical parabolic oxidation rates are observed at all stages. The initial oxidation rate is quantitatively close at high pressures to the oxidation rate at low pressures; however, the parabolic plots reveal the qualitative differences (negative curvature at high p_{O_2} noted especially on Figure 5).

From the later oxidation stages where well-behaved parabolic rates are found, we have evaluated parabolic rate constants, k_p, which are plotted in Figure 8 as a function of p_{O_2} at different temperatures. A sharp decrease in the parabolic rate constant takes place at an oxygen pressure of about 50-100 torr O_2. At low oxygen pressures (10-1 torr O_2), k_p is approximately independent of oxygen pressure. The scatter at 900 C in Figure 8 is partially due to experimental error and partially due to a real effect that will be discussed later. At high oxygen pressures it is difficult to evaluate an accurate oxygen-pressure dependence of k_p, but the results suggest a small increase of k_p with

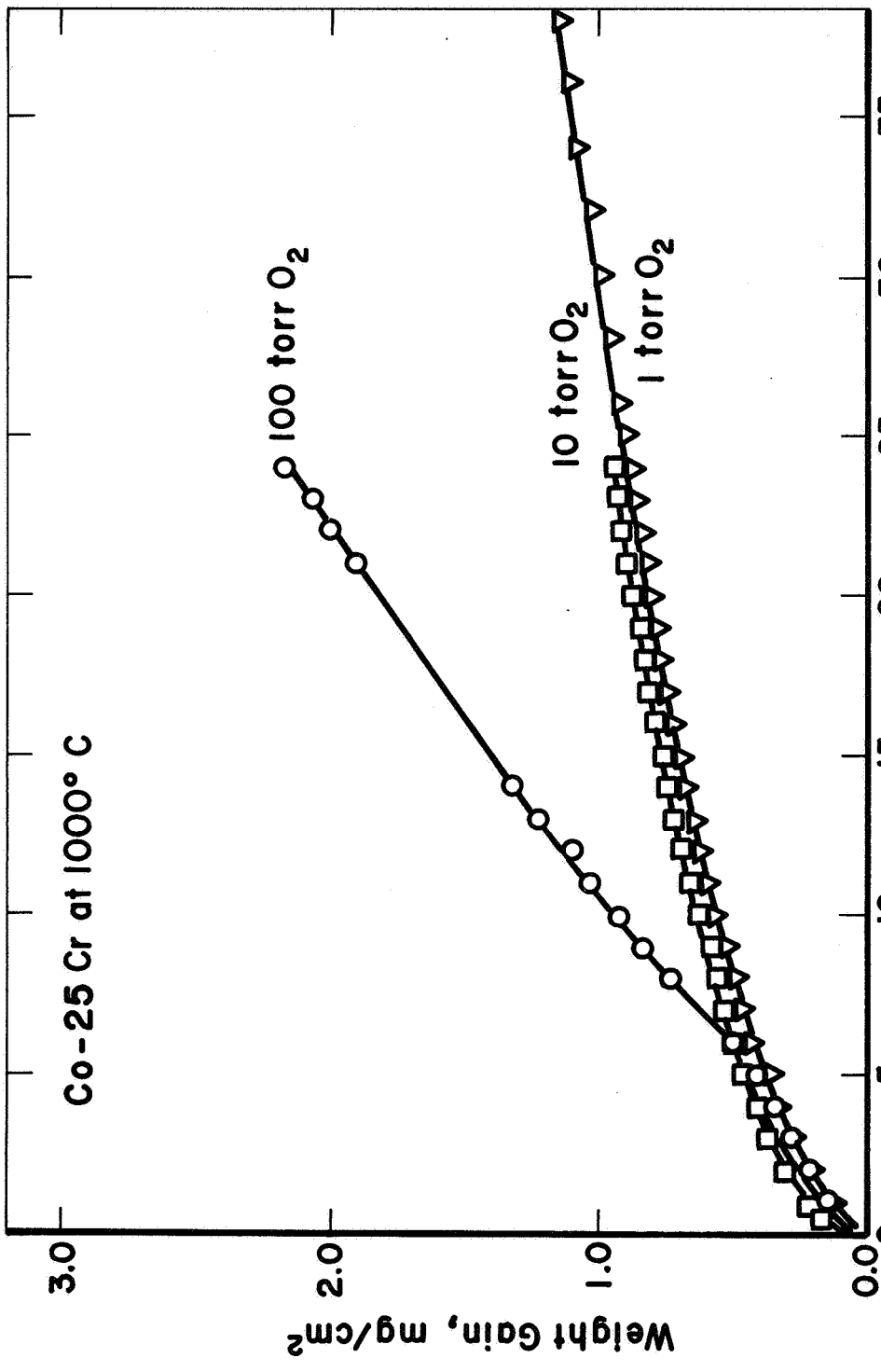

FIGURE 1. OXIDATION OF Co-25Cr ALLOY AT 1000 C IN OXYGEN AT PRESSURES FROM 1 TO 100 TORR OXYGEN

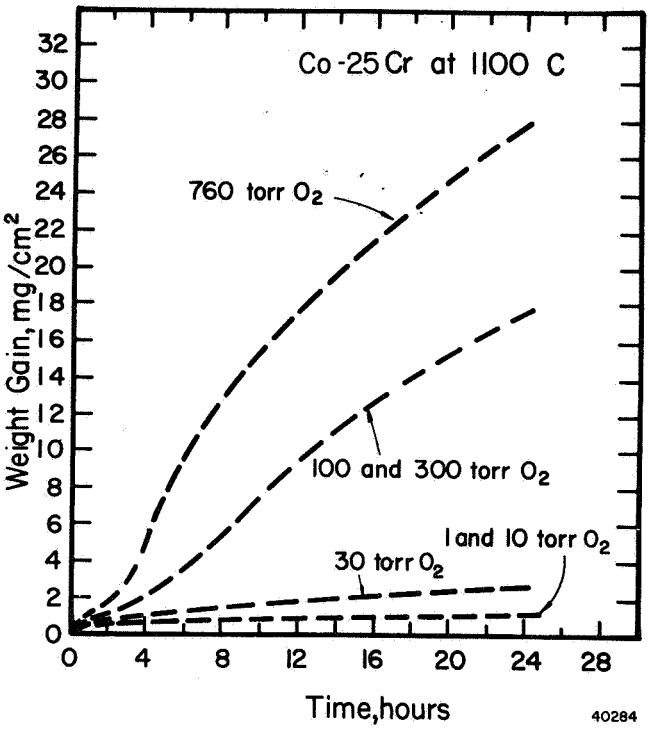

FIGURE 2. OXIDATION OF Co-25Cr ALLOY AT 1100 C IN OXYGEN AT PRESSURES FROM 1 TO 760 TORR OXYGEN

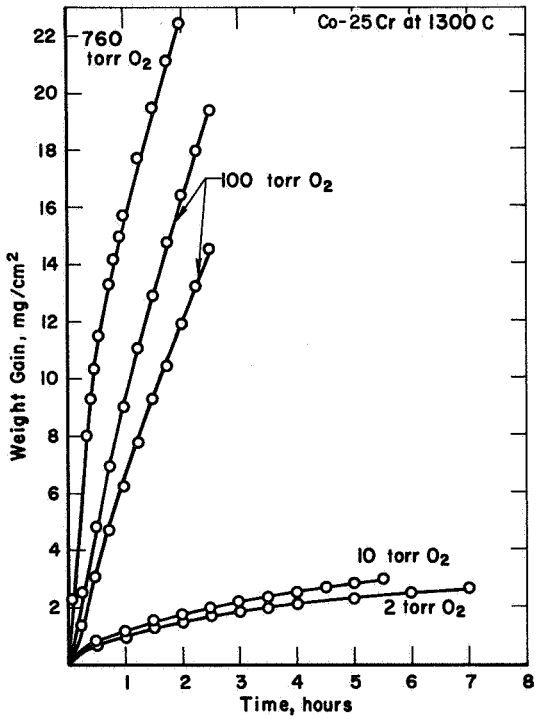

FIGURE 3. OXIDATION OF Co-25Cr ALLOY AT 1300 C IN OXYGEN AT PRESSURES FROM 2 TO 760 TORR OXYGEN

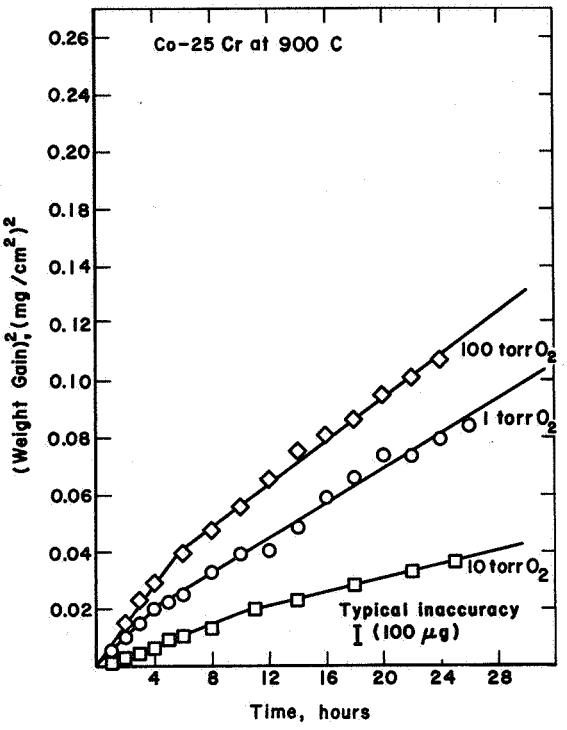

FIGURE 4. OXIDATION OF Co-25Cr ALLOY AT 900 C IN OXYGEN AT PRESSURES FROM 1 TO 100 TORR OXYGEN (PARABOLIC PLOT)

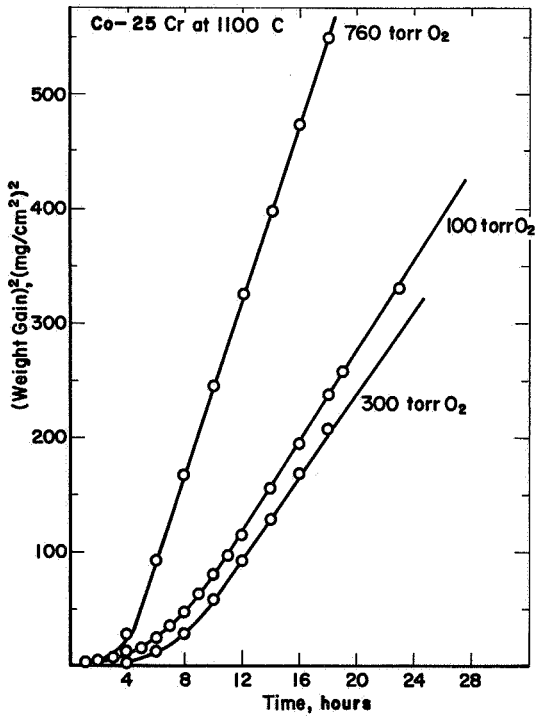

FIGURE 5. OXIDATION OF Co-25Cr ALLOY AT 1100 C IN OXYGEN AT PRESSURES FROM 100 TO 760 TORR OXYGEN (PARABOLIC PLOT)

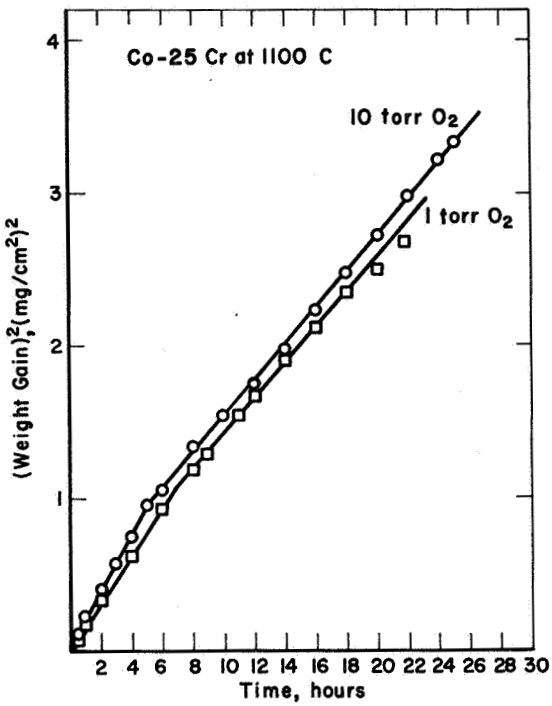

FIGURE 6. OXIDATION OF Co-25Cr ALLOY AT 1100 C IN OXYGEN AT PRESSURES OF 1 AND 10 TORR (PARABOLIC PLOT)

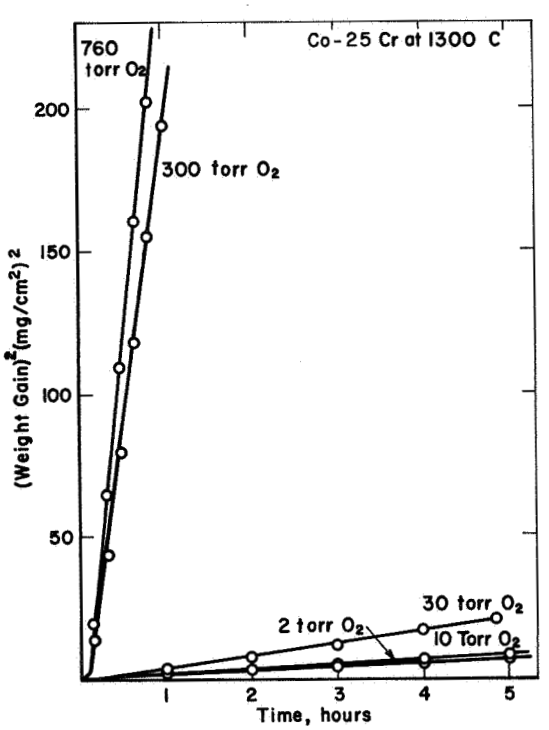

FIGURE 7. OXIDATION OF Co-25Cr ALLOY AT 1300 C IN OXYGEN AT PRESSURES FROM 2 TO 760 TORR OXYGEN (PARABOLIC PLOTS)

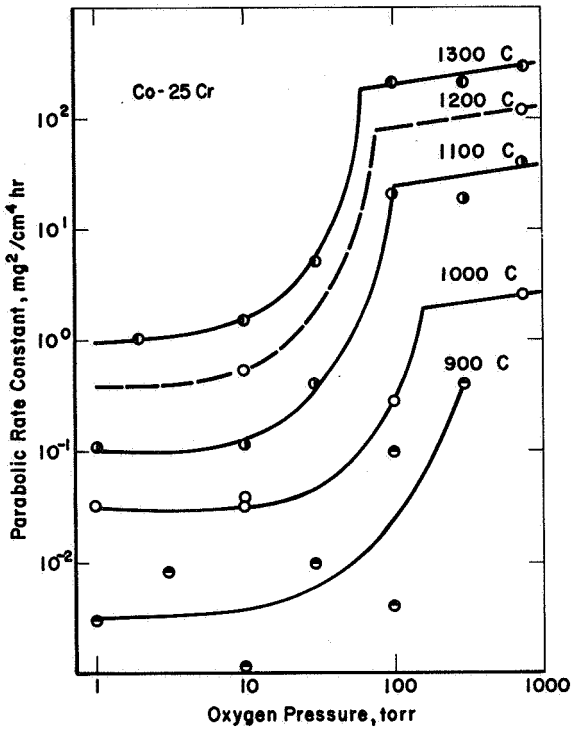

FIGURE 8. PARABOLIC RATE CONSTANT FOR OXIDATION OF Co-25Cr AS A FUNCTION OF OXYGEN PRESSURE AT TEMPERATURES FROM 900 TO 1300 C

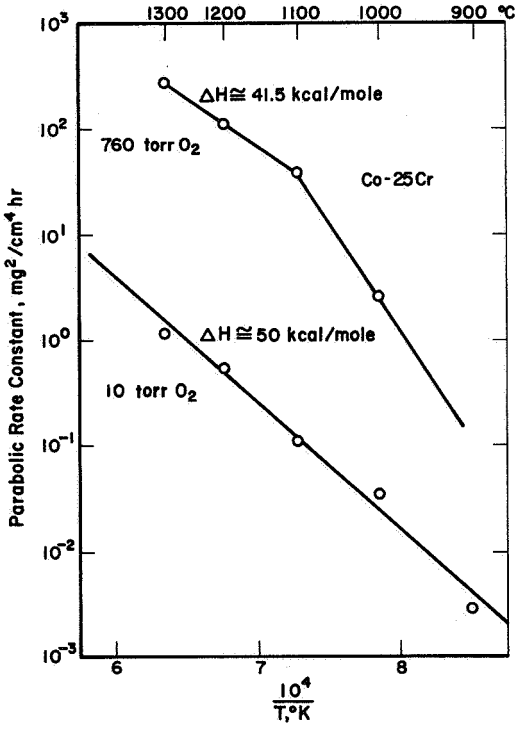

FIGURE 9. ARRHENIUS PLOT OF THE PARABOLIC RATE CONSTANT FOR OXIDATION OF Co-25Cr ALLOY AT 10 AND 760 TORR OXYGEN

oxygen pressure, which is not incompatible with a relation $k_p \propto p_{O_2}^{1/3}$ or $p_{O_2}^{1/4}$, as found for oxidation of pure cobalt and Co-10Cr.[1, 2, 3]*

In Figure 9 the parabolic rate constant at 760 torr O_2 and 10 torr O_2 is plotted as a function of $\frac{1}{T}$. The corresponding activation energies are, respectively, 41.5 kcal/mole and 50 kcal/mole. The increase in the activation energy at 760 torr ($T < 1100$) is a reflection of a change in the oxidation mechanism. The thermogravimetric results may be to some degree inaccurate, since evidence of CrO_3 evaporation was found on the hangdown wire. This was more pronounced at high p_{O_2} as expected. It was not possible to estimate this inaccuracy; however, the presence of an outer CoO layer at high p_{O_2} on Co-25Cr alloy lets us assume that this evaporation occurs only at the initial stages of oxidation.

Typical parabolic plots of the weight gain during oxidation of Co-35Cr in different oxygen partial pressures at 900 and 1100 C are given in Figures 10 and 11. The oxidation is very similar in behavior to that of Co-25Cr in low oxygen partial pressures; the oxidation is parabolic in nature; however, breaks occur after a given initial time. The parabolic rate constant, calculated beyond the breaks as in Figures 10 and 11, are given in Figure 12. No marked oxygen partial pressure dependence is noted, although a slight increase in the rate of oxidation with decreasing oxygen pressure may be observed.

RESULTS OF METALLOGRAPHIC STUDIES

Metallographic studies of oxidized specimens of Co-25Cr and Co-35Cr are difficult. Long oxidation times are needed to produce an observable scale at low oxidation temperatures. The scales spall off and must be retained by quenching in liquid metal. Because the solidified quenching metal is softer than the oxide, a metallographic preparation of the sample tends to round the polished oxide scales, making metallographic observation difficult. One must therefore go to high oxidizing temperatures for relatively long times to obtain observable scales. In Figure 13, a metallographic section of a sample of Co-25Cr alloy oxidized in air for 236 hours at 1000 C is given. Figures 14 and 15 show cross sections of samples oxidized at 1100 C in 300 torr O_2 for 14 hours and at 1300 C in 760 torr O_2 for 2 hours, respectively. The scales produced in all three cases resemble, to some degree, scales formed on the Co-10Cr alloy during oxidation.[1] The scales have a duplex structure of an outer dense layer, with large pores, and an inner layer. The details of the morphology of the inner layer differ slightly from sample to sample, depending on the oxidation atmosphere and the temperature. The outer layer consists of CoO, and the inner layer contains a large amount of spinel.

In Figure 16 a metallographic section of a sample of Co-25Cr alloy oxidized in 10 torr O_2 for 5.5 hours at 1300 C is shown. One can observe a duplex structure only in the corner, where the oxidation proceeded more intensively than in other parts of the sample. The scale on flat surfaces is no longer double-layered. Such a behavior, namely, single-layer scale on the surface of oxidized specimens, was observed whenever the oxidation was carried out at low oxygen partial pressure ($\leq$10 torr O_2). However, good metallographic pictures were difficult to produce.

---

*References are given on page 33.

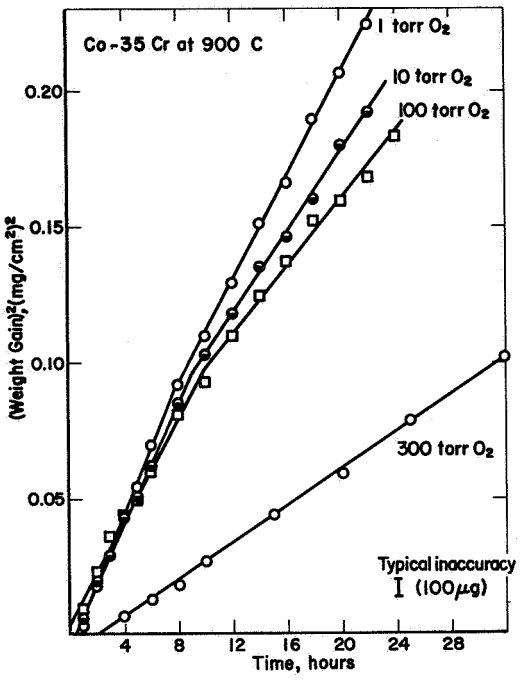

FIGURE 10. OXIDATION OF Co-35Cr ALLOY AT 900 C IN OXYGEN AT PRESSURES FROM 1 TO 300 TORR OXYGEN (PARABOLIC PLOTS)

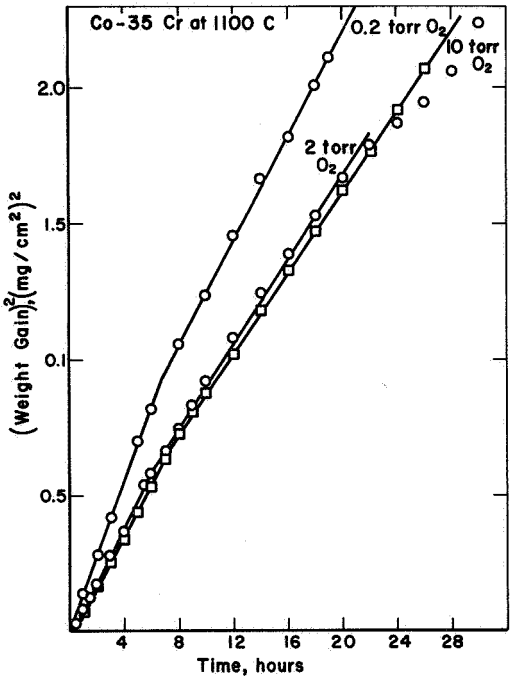

FIGURE 11. OXIDATION OF Co-35Cr ALLOY AT 1100 C IN OXYGEN AT PRESSURES FROM 0.2 TO 10 TORR OXYGEN (PARABOLIC PLOTS)

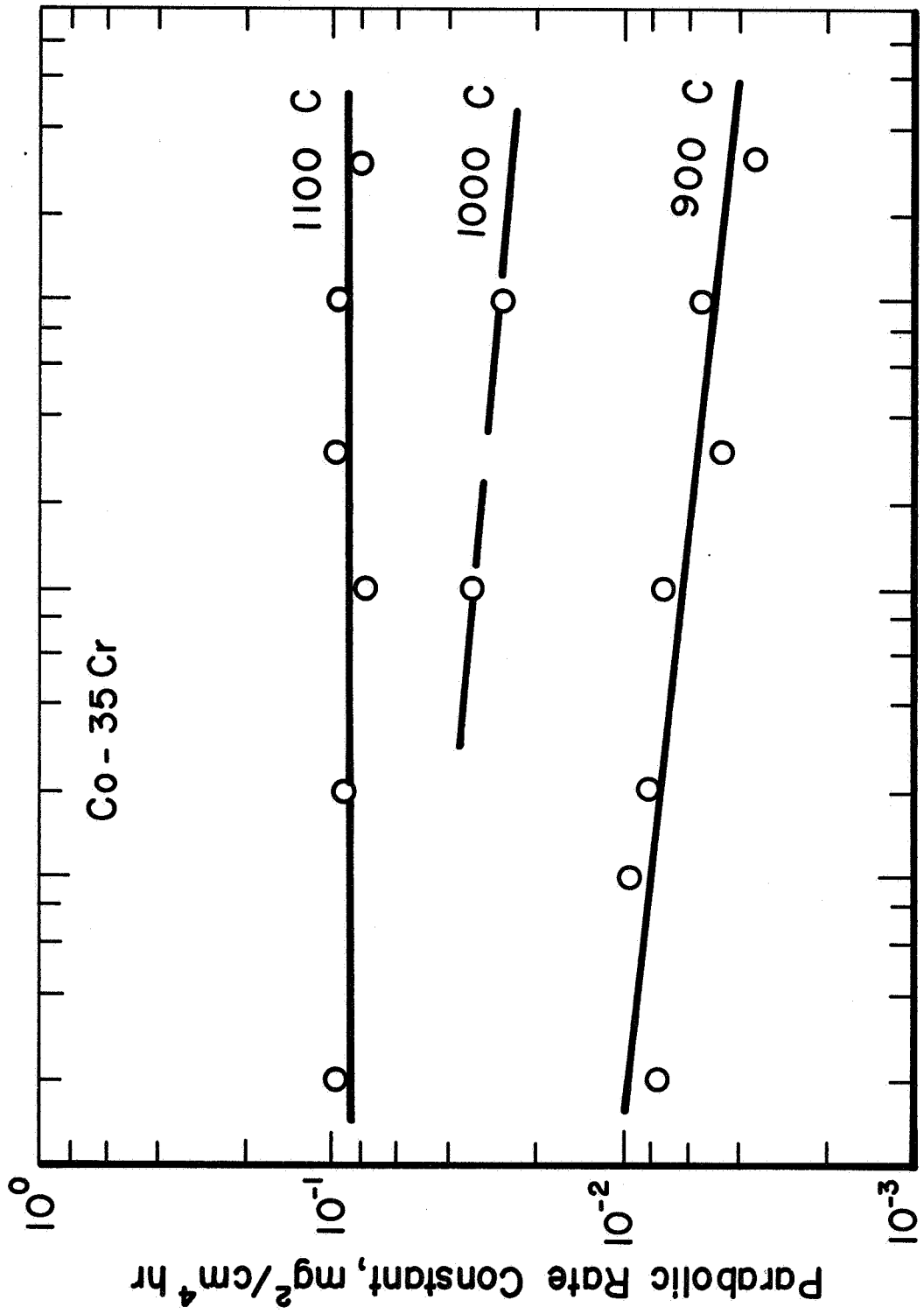

FIGURE 12. PARABOLIC RATE CONSTANT FOR OXIDATION OF Co-35Cr ALLOY AS A FUNCTION OF OXYGEN PRESSURE

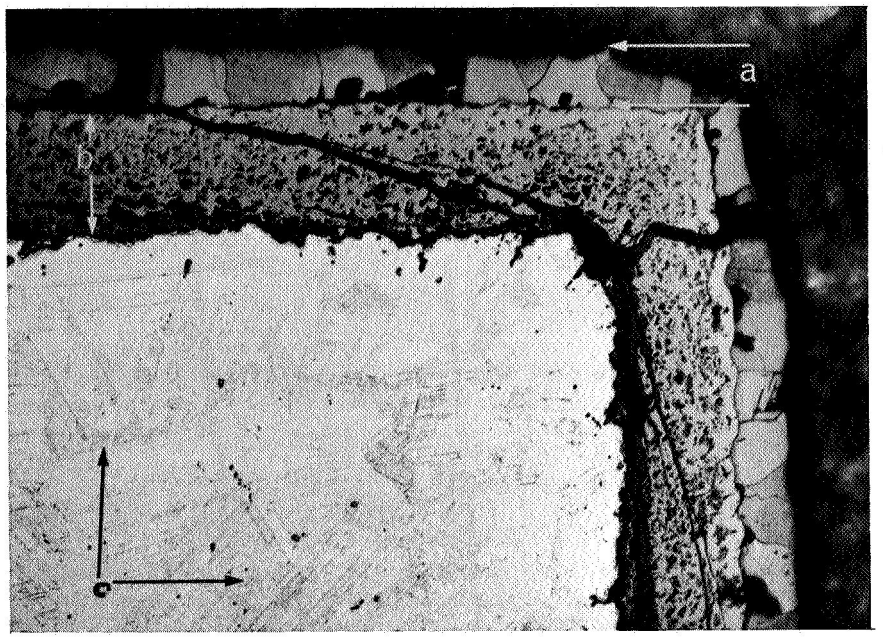

100X

FIGURE 13. METALLOGRAPHIC CROSS SECTION OF Co-25Cr ALLOY OXIDIZED AT 1000 C FOR 236 HOURS IN AIR

a. CoO outer scale; b. Inner scale (mainly spinel); c. Alloy

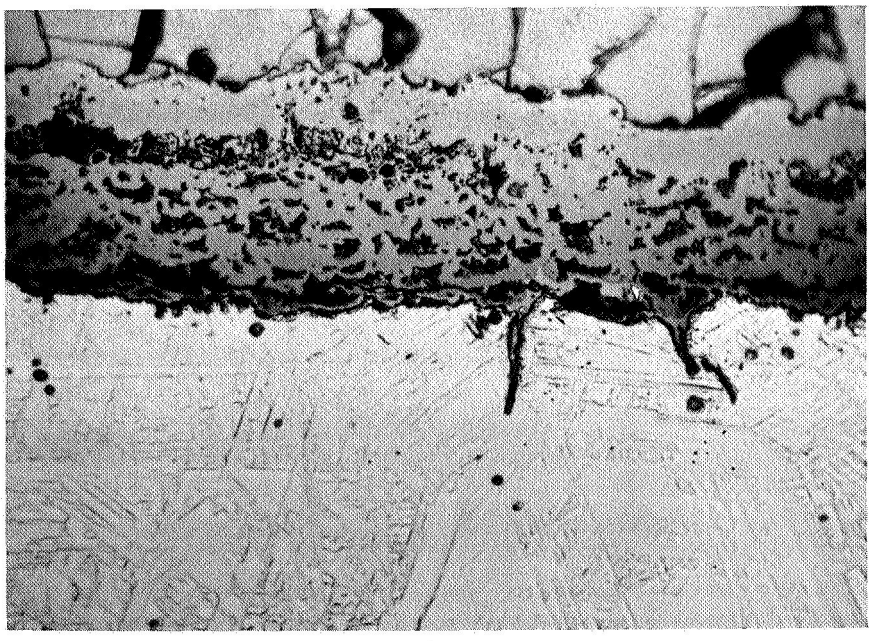

500X

FIGURE 14. METALLOGRAPHIC CROSS SECTION OF Co-25Cr ALLOY OXIDIZED FOR 14 HOURS AT 1100 C AND 300 TORR OXYGEN

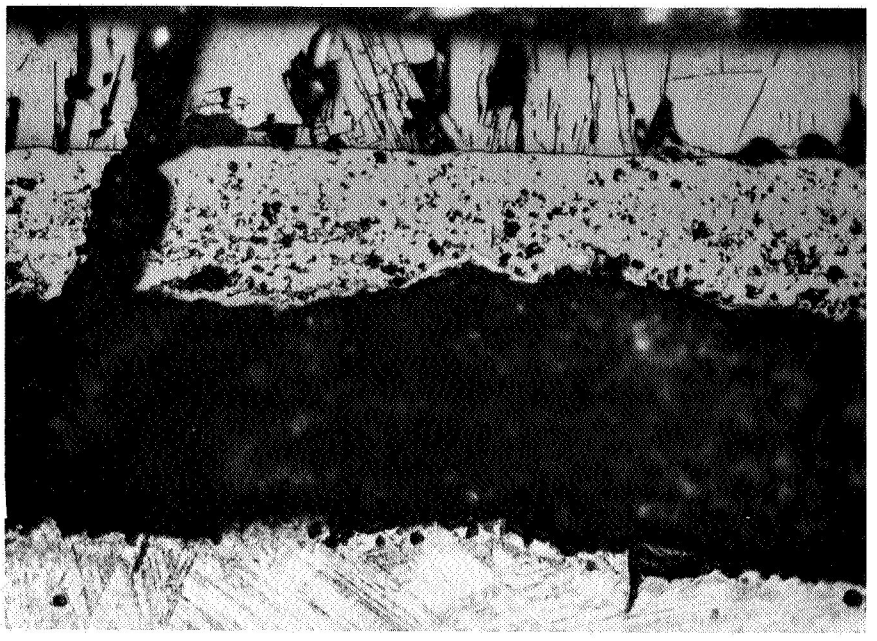

250X

FIGURE 15. METALLOGRAPHIC CROSS SECTION OF Co-25Cr ALLOY OXIDIZED FOR 2 HOURS AT 1300 C AND 760 TORR OXYGEN

250X

FIGURE 16. METALLOGRAPHIC CROSS SECTION OF Co-25Cr ALLOY OXIDIZED FOR 5.5 HOURS AT 1300 C AND 10 TORR OXYGEN

Figure 17 shows a metallographic cross section of a Co-35Cr alloy oxidized in 760 torr O_2 at 1300 C for 22 hours. Figure 18 represents a metallographic picture of the corner of the same sample. One can observe the greater extent to which oxidation has proceeded at the corner. Remnants of a duplex structure are also observed. The outer previously pure CoO scale has reacted to form spinel, and only remnants of CoO are observed, as shown in Figure 18. Figure 17 also shows discrete CoO particles on the outer surface. This feature is noted on the entire surface of the specimen oxidized at 760 torr O_2.

Figure 19 shows a cross section of a Co-35Cr alloy oxidized at 1300 C in 2 torr O_2. The oxidation at the corner is not as severe as at high oxygen pressure, and no CoO particles are observable on the surface. Figures 20 and 21 are metallographic sections of specimens oxidized at 1100 C at 30 torr O_2 and in air, respectively, while Figures 22 and 23 show corners of these specimens, respectively. All the metallographic pictures of oxidized Co-25Cr and Co-35Cr alloys revealed Cr_2O_3 inclusions in the underlying metal. Such inclusions are found also in specimens before oxidation. However, their concentration near the metal oxide interface is larger after oxidation and may be attributed to internal oxidation.

DISCUSSION

The experimental evidence suggests that mainly two oxidation processes take place in the oxidation of Co-25Cr and Co-35Cr. One mechanism governs the oxidation rate of Co-25Cr at high oxygen partial pressure. A second mechanism governs the oxidation rate for Co-25Cr at low pressures and Co-35Cr at all pressures.

The large decrease in the parabolic rate constant with decreasing oxygen pressure in the oxidation of Co-25Cr is accompanied by a drastic change in the composition and morphology of the scale. In high oxygen partial pressures, a CoO scale is formed on the outer surface of an oxidized Co-25Cr alloy. This shows that cobalt cations are transported from the metal to the outer surface. The transport is solid-state-diffusion controlled, at least in its later stages, since the oxidation at that point follows a parabolic rate law. The mechanism governing oxidation of Co-35Cr and Co-25Cr at low pressures does not involve a major transport of cobalt cations to the outer surface to form a CoO layer. One must conclude that the oxidation proceeds by a growth of spinel, which is controlled by the slower diffusion species, namely, chromium cations through a spinel scale.[2]

A detailed hypothesis for the oxidation behavior of Co-25Cr at high p_{O_2} is presented here. Since we assume that the rate-controlling step is solid-state diffusion of Co, the following equation holds:

$$\frac{dx}{dt} = \frac{k'_p A_{eff}}{x} \quad , \tag{1}$$

where x is the thickness of the scale, k'_p is a parabolic rate constant related to the measured k_p as discussed below, and A_{eff} is the effective diffusion area for Co in CoO – which is equal to the total area, A_T, minus the area A_S occupied by the spinel and the area $A_{Cr_2O_3}$ occupied by Cr_2O_3.

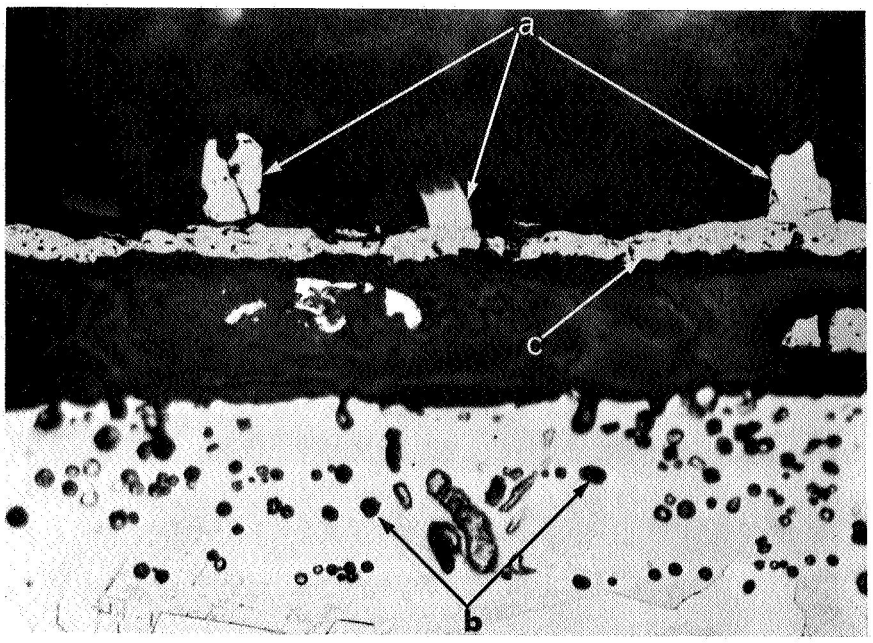

250X

FIGURE 17. METALLOGRAPHIC CROSS SECTION OF Co-35Cr ALLOY OXIDIZED FOR 22 HOURS AT 1300 C AND 760 TORR OXYGEN

a. CoO particles; b. Cr_2O_3 (internal oxide); c. Mainly $CoCr_2O_4$

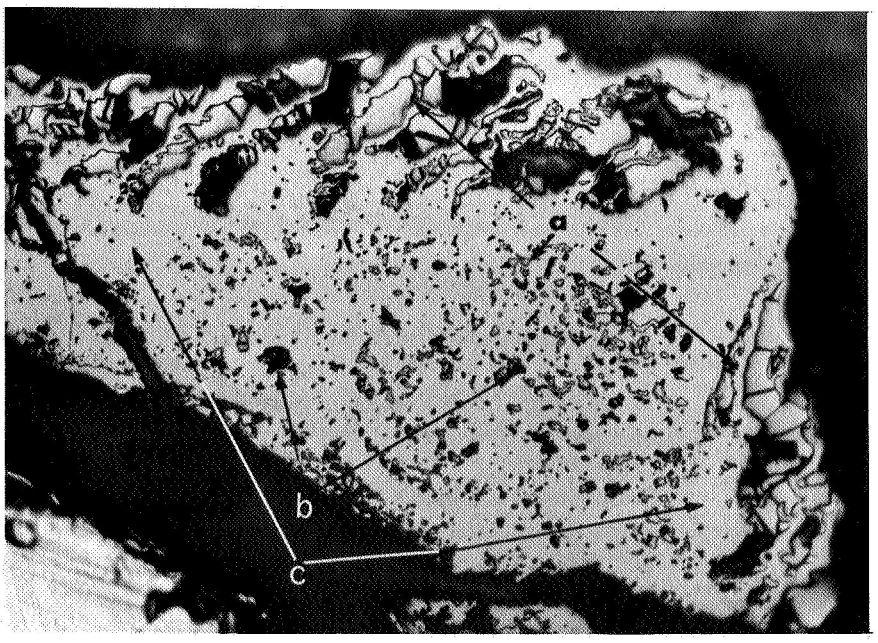

250X

FIGURE 18. CORNER OF SPECIMEN IN FIGURE 17

a. CoO inclusion; b. Cr_2O_3 and pores;
c. $CoCr_2O_4$ scale

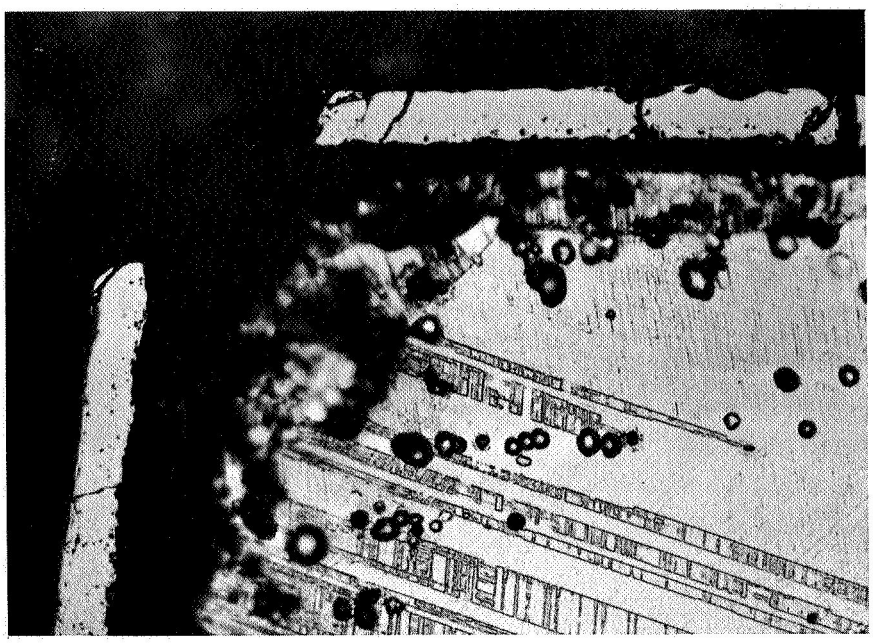

250X

FIGURE 19. METALLOGRAPHIC CROSS SECTION OF Co-35Cr ALLOY OXIDIZED FOR 22 HOURS AT 1300 C AND 2 TORR OXYGEN

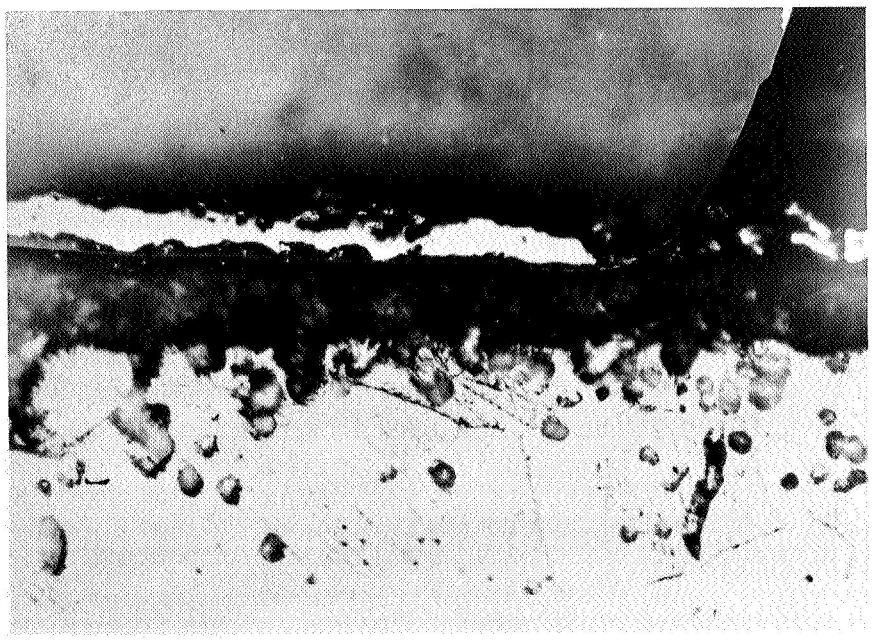

500X

FIGURE 20. METALLOGRAPHIC CROSS SECTION OF Co-35Cr ALLOY OXIDIZED FOR 68 HOURS AT 1100 C AND 30 TORR OXYGEN

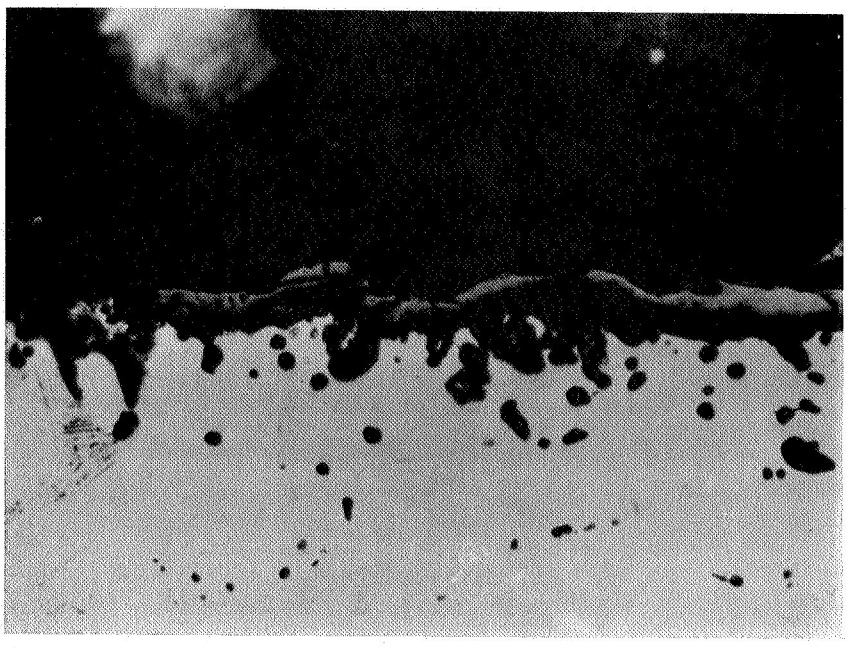

250X

FIGURE 21. METALLOGRAPHIC CROSS SECTION OF Co-35Cr ALLOY OXIDIZED FOR 246 HOURS AT 1100 C IN AIR

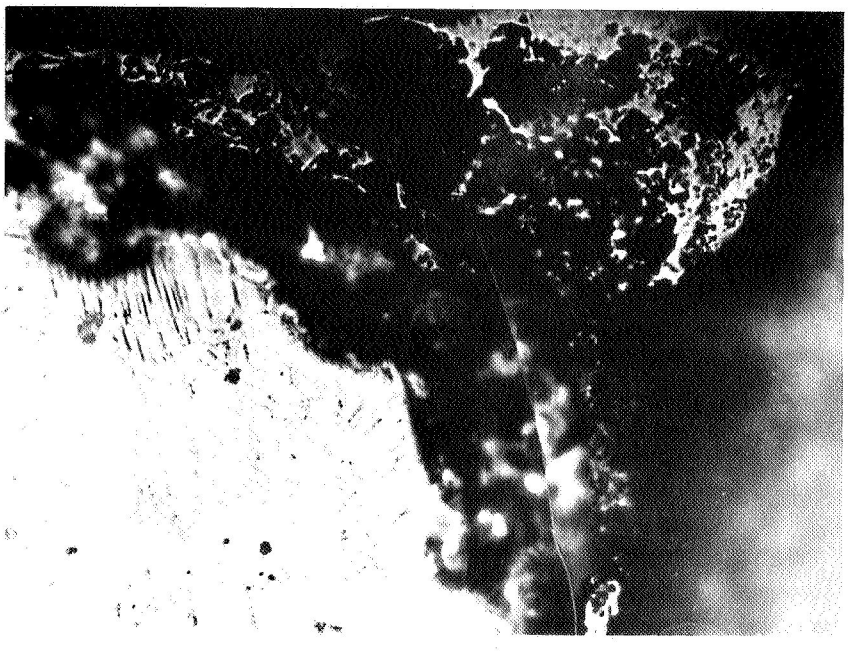

500X

FIGURE 22. CORNER OF SPECIMEN IN FIGURE 20

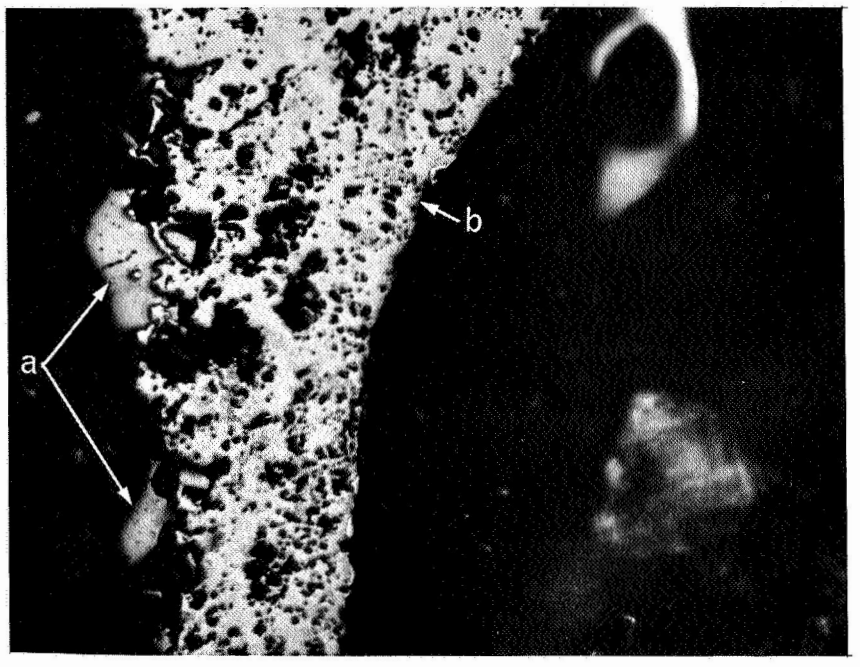

250X

FIGURE 23. CORNER OF SPECIMEN IN FIGURE 21

a. CoO particles; b. Mainly $CoCr_2O_4$

We will assume that the rate of reaction to produce spinel is proportional to the effective cross-sectional area of Cr_2O_3. This assumption is justified for the following reason: usually, creation of spinel from the two oxides is diffusion controlled and is determined by the rate of interdiffusion of the two oxides Cr_2O_3 and CoO, which in turn depends on the geometry of the two oxides. In our case we have a flow of Co cation in a given direction due to a Co vacancy gradient, and Cr_2O_3 is present as fine particles.

The rate of spinel formation will be proportional to the area of reaction and inversely proportional to the depth of interpenetration. Since Cr_2O_3 appears as very fine particles, we disregard the depth of interpenetration in the following analysis. Also, we are interested in the rate at which the area of the spinel perpendicular to the Co flow increases, which is almost independent of the depth of penetration. We therefore postulate that the following equation holds:

$$\frac{dA_s}{dt} = kA_{Cr_2O_3} = k(A_o - \alpha A_s) \quad , \tag{2}$$

where

A_s = spinel cross section

$A_{Cr_2O_3}$ = Cr_2O_3 cross section

A_o = an initial cross section of Cr_2O_3 (mainly due to preferential oxidation of Cr in the beginning of a run when the specimen is in a vacuum of 10^{-5} torr)

α = a factor that relates the effective cross-sectional area of the spinel formed to the cross-sectional area of Cr_2O_3 consumed

K = the surface rate constant for the formation of spinel.

Rearranging Equation (2), we have

$$\frac{dA_s}{A_o - \alpha A_s} = kdt \quad . \tag{3}$$

Integration of this equation yields

$$\frac{-\log A_o - \alpha A_s}{\alpha} = kt + \text{const} \quad . \tag{4}$$

The integration constant is calculated from the following initial conditions: t = O, A_s = O, with these conditions, the solution of Equation (3) is

$$\frac{1}{\alpha}\log\left(\frac{A_o - \alpha A_s}{A_o}\right) = -kt \tag{5}$$

$$A_o - \alpha A_s = A_o e^{-\alpha kt} \quad . \tag{6}$$

Rearranging Equation (6), we have

$$\frac{A_o(1 - e^{-\alpha kt})}{\alpha} = A_s \quad . \tag{7}$$

From Equation (2), we have $A_{Cr_2O_3} = A_o - \alpha A_s$ and, with Equation (7),

$$A_{Cr_2O_3} = A_o - A_o(1-e^{-\alpha kt}) = A_o e^{-\alpha kt} \quad . \tag{8}$$

As pointed out above, the effective area for Co diffusion is given by $A_{eff} = A_T - A_s - A_{Cr_2O_3}$, where A_T is the total area of the specimen.

Substituting the expressions for A_s and $A_{Cr_2O_3}$ given in Equations (7) and (8), we have

$$A_{eff} = A_T - \frac{A_o(1 - e^{-\alpha kt}) + \alpha A_o e^{-\alpha kt}}{\alpha} \quad ,$$

or

$$A_{eff} = A_T - \frac{A_o}{\alpha} - \frac{\alpha - 1}{\alpha} A_o e^{-\alpha kt} \quad . \tag{9}$$

Substituting this value A_{eff} in Equation (1), we have

$$\frac{dx}{dt} = \frac{k_p' \left\{ A_T - \frac{A_o}{\alpha} - \frac{\alpha - 1}{\alpha} A_o e^{-\alpha kt} \right\}}{x} \quad . \tag{10}$$

Integration of Equation (10) yields

$$x^2 = k_p' \left(A_T - \frac{A_o}{\alpha} \right) t + A_o \frac{\alpha - 1}{\alpha^2 k} e^{-\alpha kt} + \text{const}'' \quad . \tag{11}$$

The integration constant is calculated from the following initial conditions: $t = 0$, $x = 0$; therefore $\text{const}'' = -\frac{\alpha - 1}{\alpha^2 k} A_o$.

The weight gain, ΔW, and the thickness of the scale, x, are related by

$$\Delta W = x A_T \rho \quad , \tag{12}$$

where ρ is a mean density of the scale assumed constant with time, which is probably true since the ratio of the inner- and outer-layer thicknesses is constant (Table 1).

TABLE 1. THICKNESS OF INNER AND OUTER LAYERS OF SPECIMENS OXIDIZED IN AIR AT 1100 C FOR DIFFERENT PERIODS

	Oxidation Period, hours		
	1	6.5	19
Thickness of Inner Layer, mm	0.01	0.034	0.1
Thickness of Outer Layer, mm	0.006	0.02	0.06
Ratio of Layer Thicknesses, inner/outer	1.67	1.7	1.67

We therefore have the relation

$$x^2\rho^2 = \left(\frac{\Delta W}{A_T}\right)^2 = \rho^2\left[k_p'\left(A_T - \frac{A_o}{\alpha}\right)t - A_o\frac{\alpha - 1}{\alpha^2 k} + A_o\frac{\alpha - 1}{\alpha^2 k}e^{-\alpha k t}\right], \qquad (13)$$

or

$$\left(\frac{\Delta W}{A_T}\right)^2 = k_p t - B + Be^{-\alpha k t}, \qquad (14)$$

where $k_p = k_p'\rho^2\left(A_T - \frac{A_o}{\alpha}\right)$ and $B = A_o\rho^2\frac{\alpha - 1}{\alpha^2 k}$. We see that the square of the weight gain can be represented by the sum of a straight line, $k_p t - B$, and an exponential function, $Be^{-\alpha k t}$. To show that our experimental results yield such a behavior, Figure 24 was drawn in the following way: the straight portion of a plot of $\left(\frac{\Delta W}{A_T}\right)^2$ versus time was extrapolated to "negative weight gain" (that line represents the equation $\left(\frac{\Delta W}{A_T}\right)^2 = k_p t - B$); the difference between the straight line values and the experimental values provides a plot of the "deviations from parabolic behavior" ($B e^{-\alpha k t}$). The last values in turn are normalized (divided by B) and their logarithms are plotted in Figure 25 as functions of t to show the exponential behavior of the deviation from parabolic behavior. In Figure 25 a family of such curves yields straight lines, which prove that the nature of the deviation from parabolic behavior is exponential.

The value of α is difficult to estimate, since it does not depend only on the bulk ratio of Cr_2O_3 and the spinel; the morphology of Cr_2O_3 formation is an important factor. Since Cr_2O_3 is formed as finely divided particles, we assume that the total cross-sectional area of Cr_2O_3 includes also the microporosity involved. This porosity can be enhanced at high pO_2 by evaporation of CrO_3. The formation of spinel results in a smaller area then the original porous Cr_2O_3; thus, α is larger than 1. The transition to very low rates of oxidation at low oxygen partial pressure may involve two factors. The first is a gradual change in the morphology of Cr_2O_3 so that $\alpha \leq 1$. That change may be due to a decreasing rate of outward migration of Co, and to less

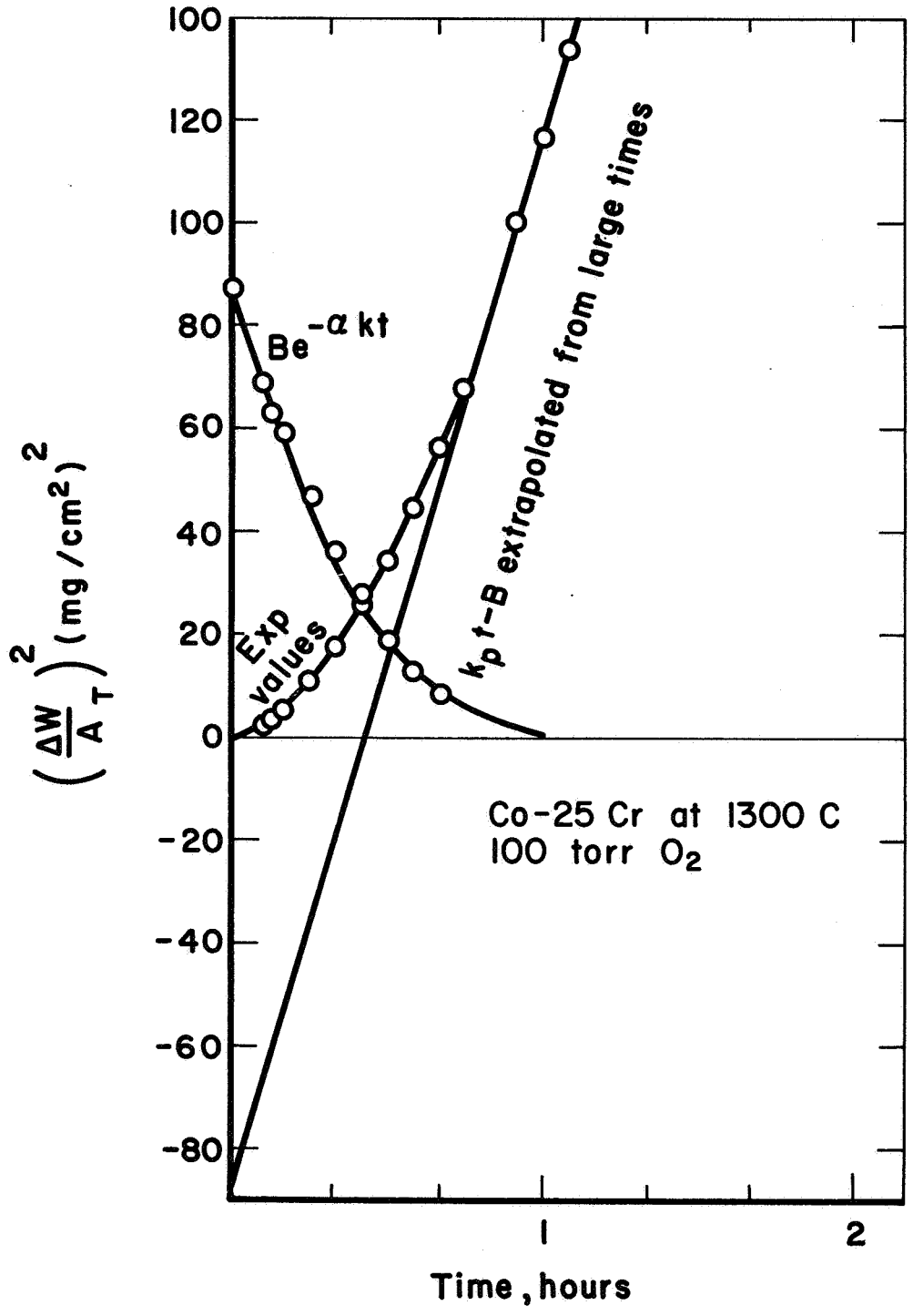

FIGURE 24. GRAPHIC REPRESENTATION OF THE CALCULATION OF THE DEVIATION FROM PARABOLIC BEHAVIOR FOR THE OXIDATION OF Co-25Cr AT HIGH OXYGEN PRESSURES

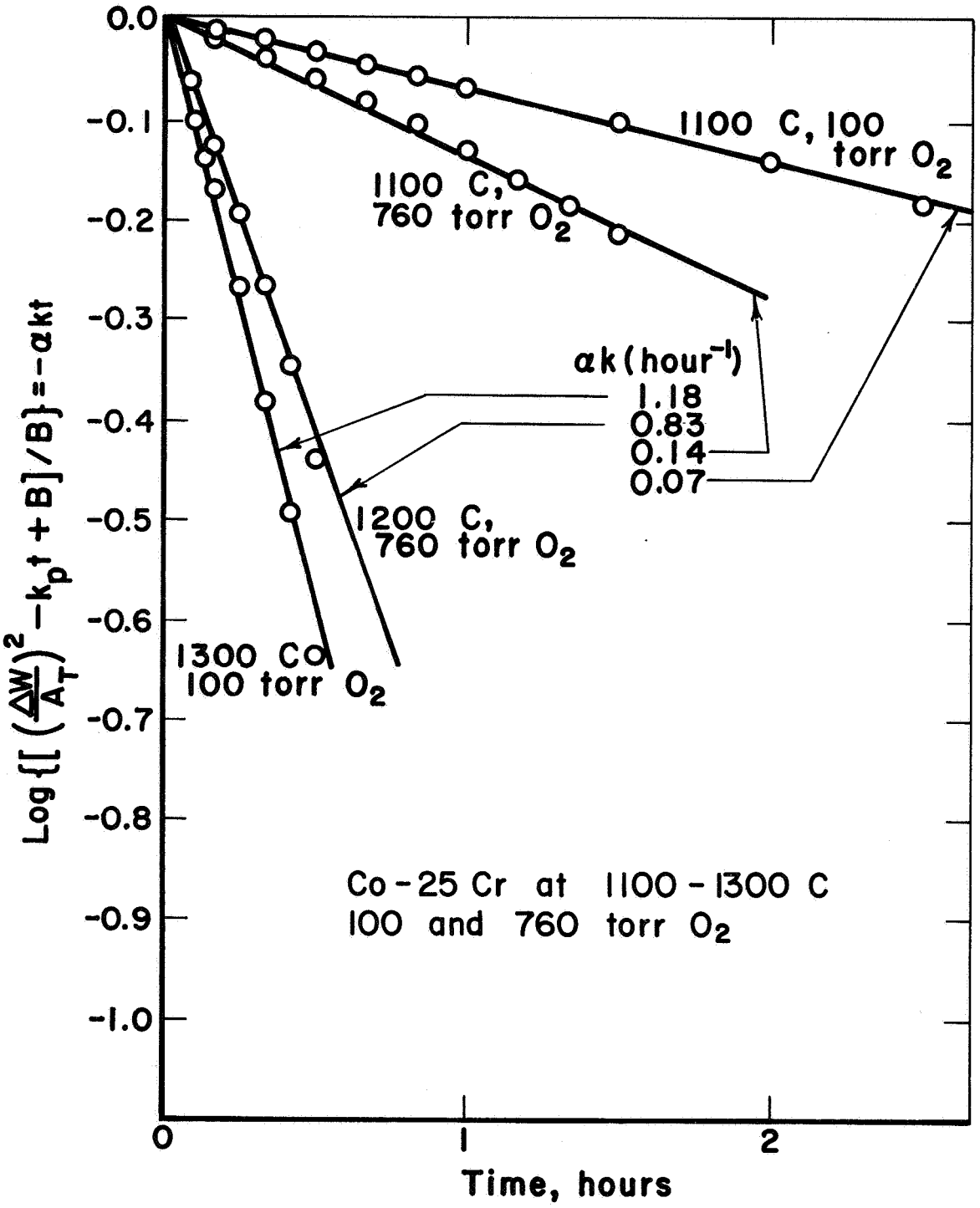

FIGURE 25. NORMALIZED DEVIATION FROM PARABOLIC BEHAVIOR FOR Co-25Cr ALLOYS OXIDIZED AT TEMPERATURES BETWEEN 1100 AND 1300 C AT HIGH OXYGEN PRESSURES

CrO_3 evaporation. That decrease in α will produce a relatively larger spinel area, and eventually, the spinel will close all channels for Co migration. A second factor is the possibility that $\alpha A_s = A_o$; this will result in the mathematical failure of Equation (3), and is physically the limiting case $\alpha = 1$.

The value of A_o is a function of too many unknowns to try to draw many conclusions from its behavior. However, we know that, before running a test, the specimen is held at temperature in a vacuum of 10^{-4} to 10^{-5} torr for a short period of time. It is highly possible that at these pressures preferential oxidation of Cr occurs; the longer this holding time, the larger is A_o and the larger are the possible deviations from parabolic oxidation rate. To prove this point, a few specimens were oxidized at 1300 C, trying to cut down the time during which preoxidation might occur. Results of these tests are shown in Figure 26 along with other runs; we see that, with short holding times, the oxidation is almost perfectly parabolic.

From Equations (13) and (14), we see that the measured parabolic rate constant k_p depends on A_o, which could explain the spread sometimes observed in the oxidation rate of Co-25Cr.

Metallographic evidence supporting the above mechanism is found in Figures 27-31. These figures show different areas in the scale produced by oxidizing a Co-25Cr specimen at 1300 C in 300 torr O_2. The outer layer (Figure 28) is very similar to the outer layer obtained on Co-10Cr alloy under similar conditions (Figure 32). At the interface between the outer layer and inner layer (Figure 29), one can see some CoO grain surrounded by $CoCr_2O_4$. The inner layer near this interface is almost exclusively $CoCr_2O_4$, with small inclusions of CoO. These inclusions are actually channels that connect the outer layer and inner layer; however, the tapering of the sample hides this special behavior. Inside the inner layer, the size of these CoO channels is larger, and some unreacted Cr_2O_3 is observed (Figures 30 and 31). The situation is simplified in Figure 33. Figure 33a shows the schematic situation before oxidation begins. A thin, probably noncontinuous film of Cr_2O_3 was formed due to preferential oxidation at very low pressures. This film forms the first network for the spinel formation and determines the parameter A_o. Its morphology determines the parameter α. During the initial nonparabolic stage, four processes may occur simultaneously (1) oxidation of cobalt, (2) internal oxidation of chromium, (3) evaporation of CrO_3, and (4) interaction of Cr_2O_3 and CoO to form spinel. The last reaction decreases the Cr_2O_3 area and increases the yield area; however, the total blocked area is decreased. The situation is illustrated in Figure 33b. In Figure 33c, the effective cross-sectional area, A_{eff}, is stabilized with a value $A_{eff} = A_T - \frac{A_o}{\alpha}$, and the nonparabolic stage ends. In Figure 33d, the growth of scale is illustrated for the parabolic stage, in which the rate-controlling process is Co diffusion through the CoO channels in the inner layer and the smallest CoO area perpendicular to the diffusion path is constant.

It is clear that $A_T - \frac{A_o}{\alpha}$ must be of the order of $10^{-3}A_T$ for the low oxygen partial pressure mechanism to take over, since the diffusion rates of Co and Cr cations in the spinel are three orders of magnitude less than that of Co in CoO. Figure 28 shows that the channels' cross sections provide a large enough area, still, to compete with the outward spinel growth.

The oxidation mechanisms of Co-25Cr at low oxygen pressure and of Co-35Cr at all pressures involve the closing of the channels completely, so that outward migration of Co as CoO builds on the outer surface is no longer possible. Since $CoCr_2O_4$ is

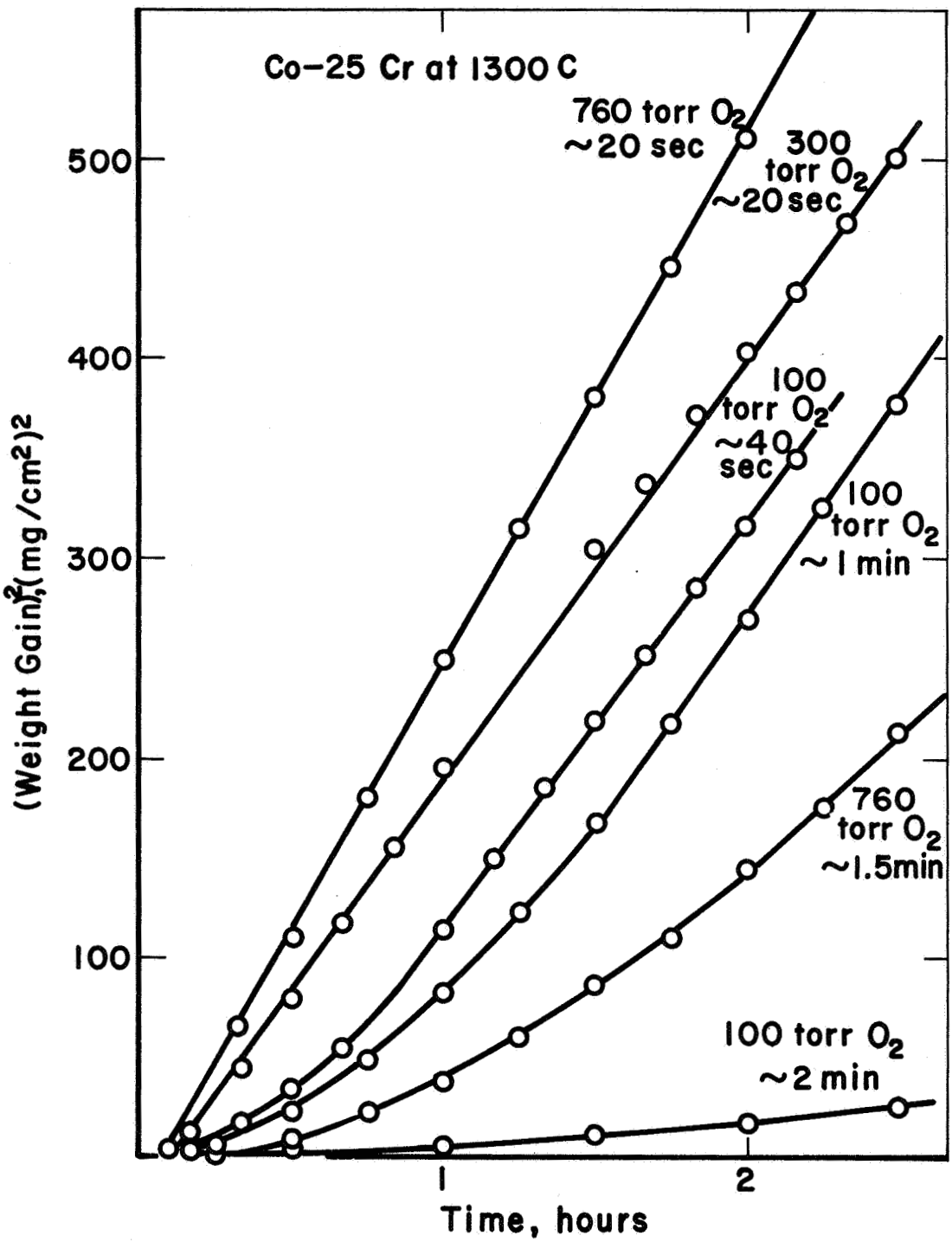

FIGURE 26. OXIDATION OF Co-25Cr ALLOYS AT 1300 C IN OXYGEN AT PRESSURES FROM 100 TO 760 TORR

Comparison of weight-gain curves of specimens that differ in their preoxidation time.

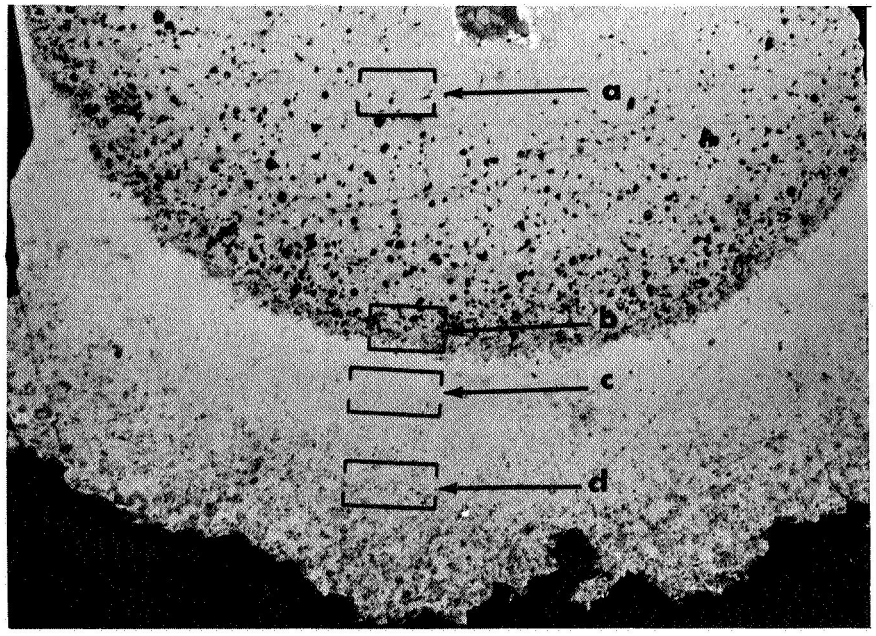

25X

FIGURE 27. METALLOGRAPHIC TAPERED CROSS SECTION OF SCALE OF Co-25Cr ALLOY OXIDIZED FOR 3 HOURS AT 1300 C AND 300 TORR OXYGEN

a. See Figure 28 (outer layer); b. see Figure 29 (inner/outer layer boundary circular due to bending of scale on peeling); c. see Figure 30 (inner layer); d. see Figure 31 (inner layer).

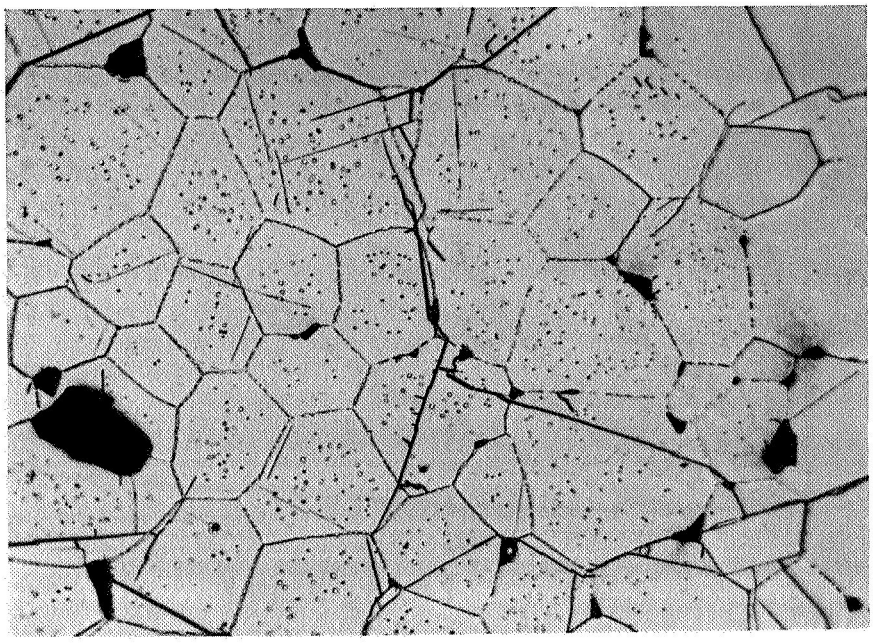

250X

FIGURE 28. SPECIMEN IN FIGURE 27 - AREA A

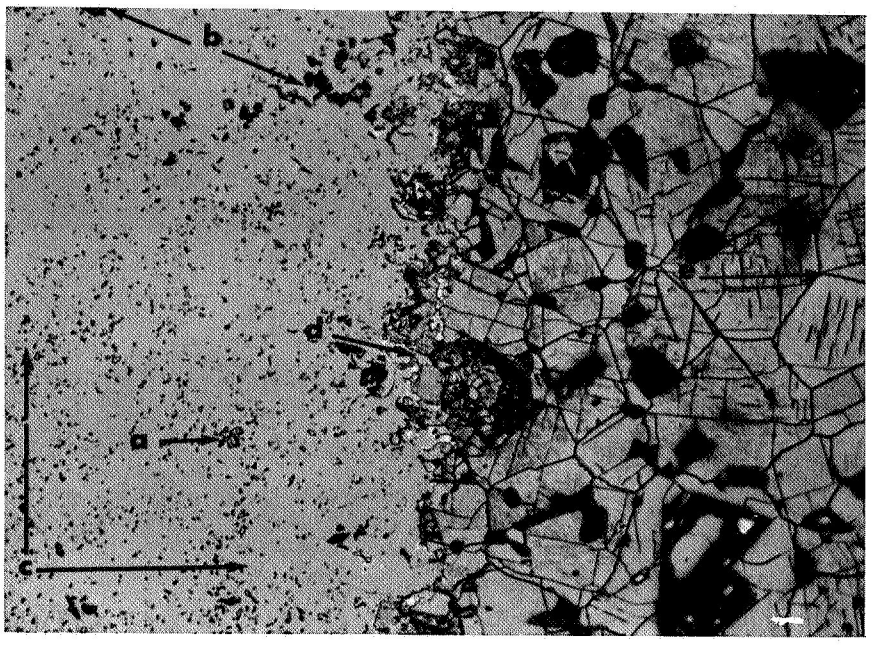

250X

FIGURE 29. SPECIMEN IN FIGURE 27 - AREA B

a. CoO inclusion; b. Cr_2O_3 and pores; c. $CoCr_2O_3$ scale; d. $CoCr_2O_4$ enclosed by CoO; e. CoO outer scale

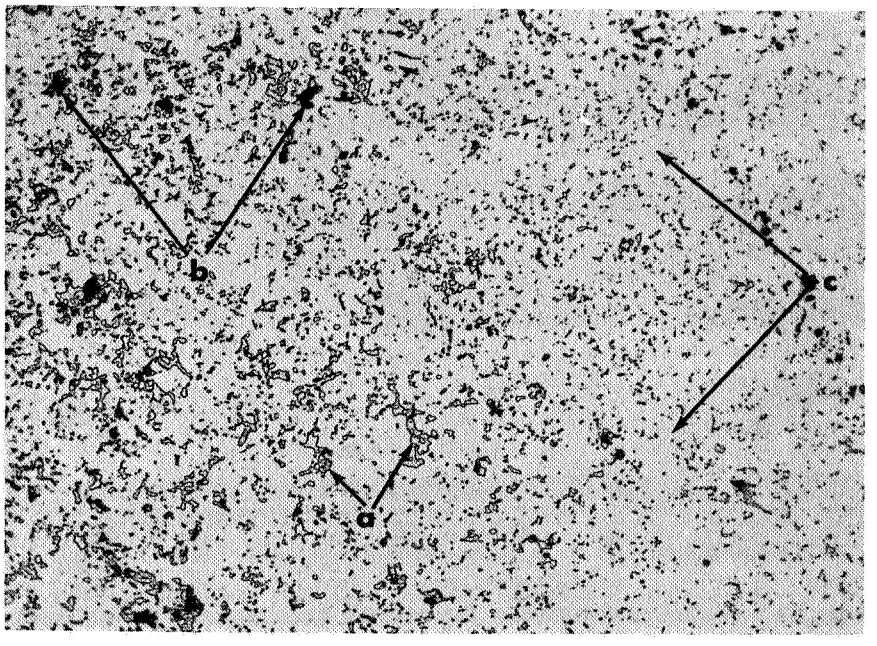

250X

FIGURE 30. SPECIMEN IN FIGURE 27 - AREA C

a. Co inclusion; b. Cr_2O_3 and pores; c. $CoCr_2O_4$ body

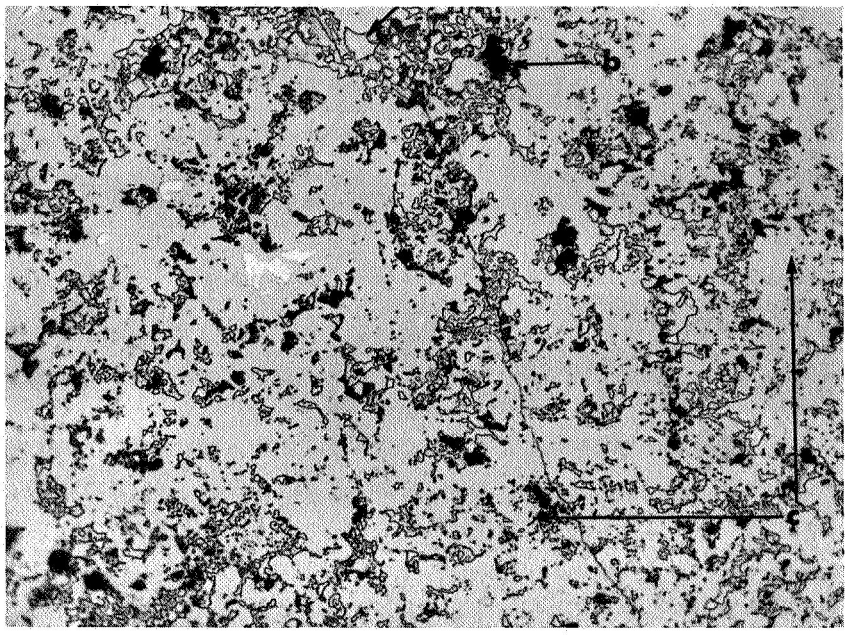

FIGURE 31. SPECIMEN IN FIGURE 27 - AREA D

a. CoO channels; b. Cr_2O_3;
c. $CoCr_2O_4$

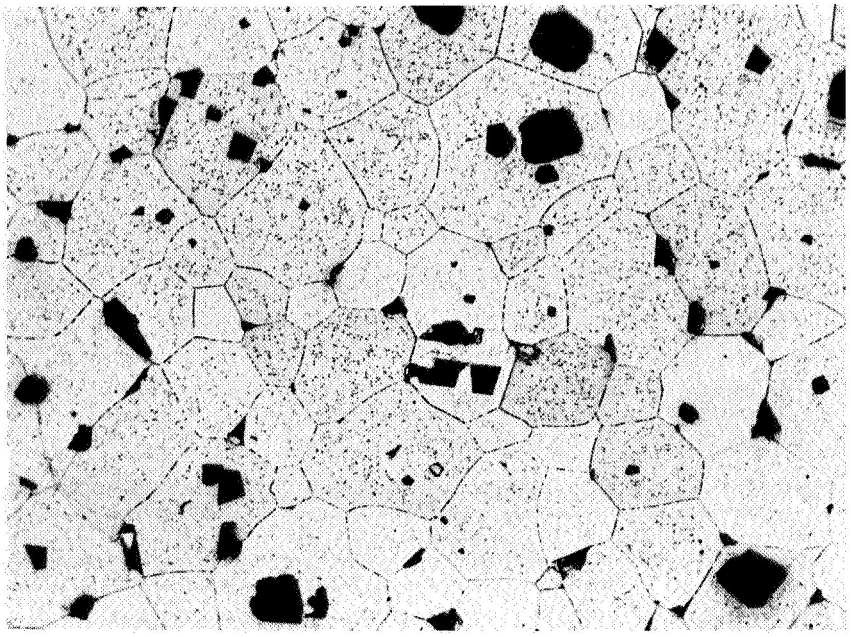

FIGURE 32. METALLOGRAPHIC TAPERED CROSS SECTION OF SCALE OF Co-10Cr ALLOY OXIDIZED FOR 3-1/2 HOURS AT 1200 C AND 100 TORR OXYGEN

Outer CoO layer

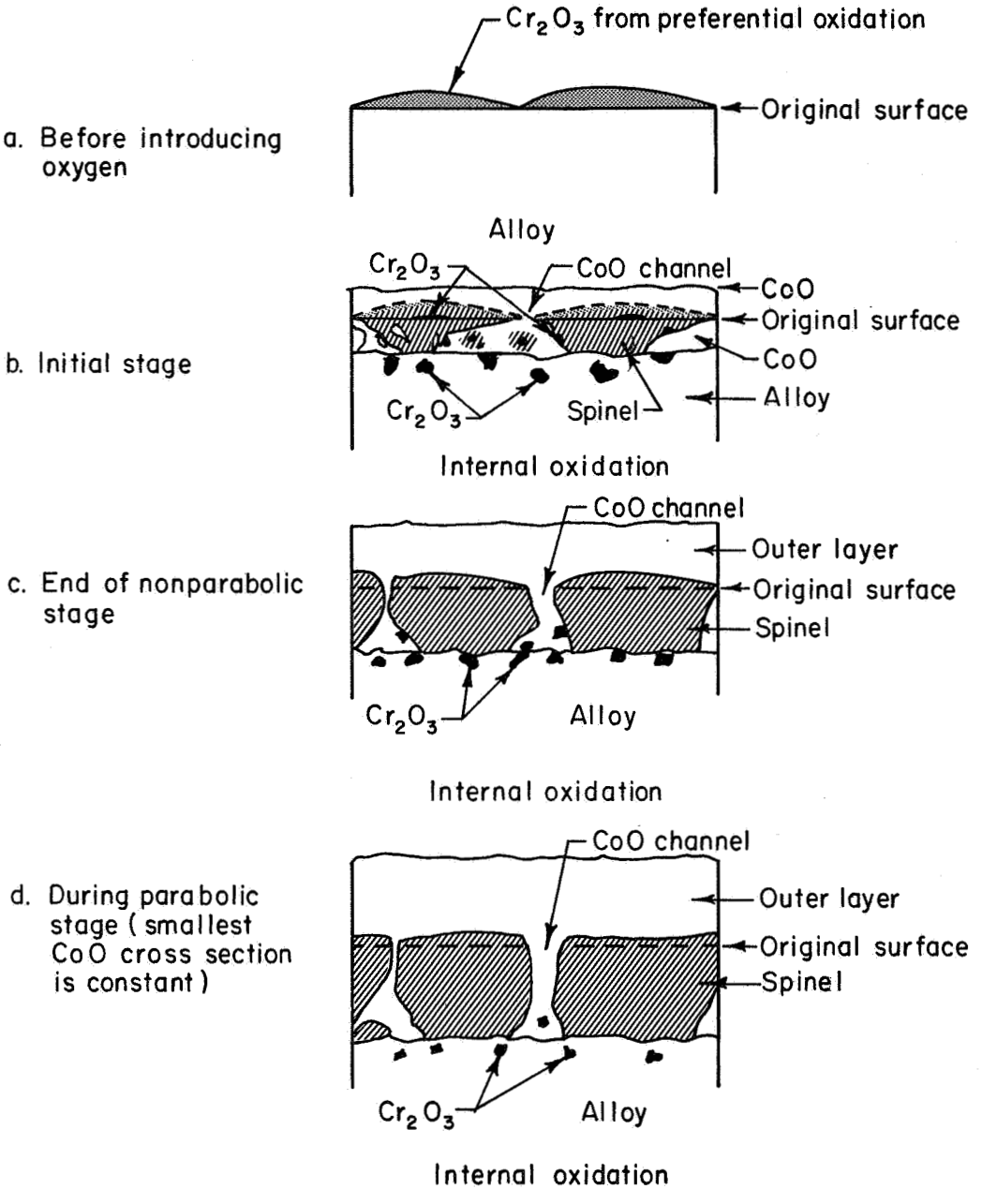

FIGURE 33. SCHEMATIC DISTRIBUTION OF THE DIFFERENT COMPONENTS IN THE SCALE OF Co-25Cr ALLOY OXIDIZED AT HIGH PRESSURES

thermodynamically more stable than CoO, decomposition of $CoCr_2O_4$ to produce a growing outer CoO layer is improbable. The rate-controlling process is determined in this case by the migration of Cr cations in $CoCr_2O_4$, resulting in an outgrowing spinel layer. This is because the diffusion rate of Cr^{3+} in the spinel is lower than that of Co^{2+} in the spinel.

The transition between the two mechanisms discussed here (Co^{2+} diffusion in CoO channels at high pressure, and Cr^{3+} diffusion in $CoCr_2O_4$ bulk at low pressure for the oxidation of Co-35Cr involves a change in the morphology of the spinel formation, which mathematically is represented by the parameters α and, to a much smaller degree, A_o. If the parameter α becomes smaller than 1, the preexponent in Equation (14) becomes negative, the initial parabolic oxidation curves must have a positive curvature, and parabolic parts of the weight gain have the form

$$\left(\frac{\Delta W}{A_T}\right)^2_{(\text{parabolic})} = k_p t + B \quad . \tag{15}$$

The total weight gain has the form

$$\left(\frac{\Delta W}{A_T}\right)^2_{\text{total}} = k_p t + B - B e^{-\alpha k t} \quad , \tag{16}$$

where B is $\rho^2 \frac{1-\alpha}{\alpha^2 k} A_o$.

The term k_p will now be the parabolic rate constant for the mechanisms of spinel outgrowth. To show the validity of this mechanism, an analysis of the oxidation-rate curve at low pressure was performed. A representative curve is given in Figure 34 and the normalized exponential parts are given in Figure 35. The exponential character of the deviation from parabolic behavior is well shown.

Comment on the Oxidation of Co-35Cr Alloy

It appears that the oxidation of Co-35Cr as a general tendency increased with decreasing oxygen pressure. This is perhaps even more marked for the weight-gain curves than for k_p. This is, of course, difficult to explain on the basis of the mechanism involving formation of spinel $CoCr_2O_4$ only.

It is suggested that matters are more complicated and, specifically, that we probably have to take into account preferential oxidation of Cr to form Cr_2O_3. This will become increasingly important with lower oxygen pressure and, as we decrease the oxygen pressure, the scale will consist of an increasingly larger fraction of Cr_2O_3. As diffusion of Cr^{3+} is appreciably higher in Cr_2O_3 than in $CoCr_2O_4$, we will qualitatively obtain the observed oxygen-pressure dependence.

If this is the case (experimental confirmation is needed), it will represent a very interesting phenomenon and provide an interesting model. To our knowledge, this has not been previously described in the literature, perhaps because increasing rates of reaction with decreasing pressures are highly unusual.

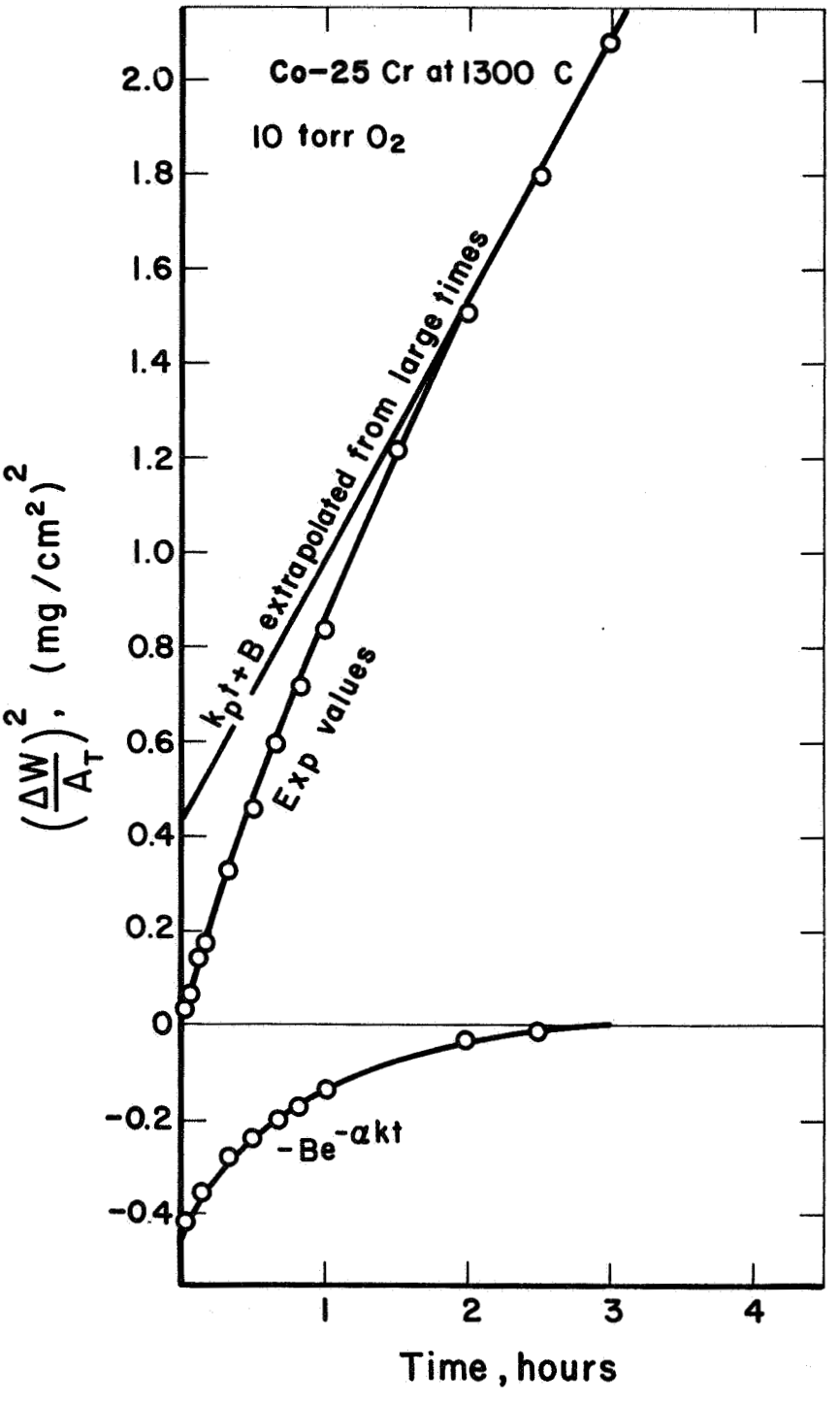

FIGURE 34. GRAPHIC REPRESENTATION OF THE CALCULATION OF THE DEVIATION FROM PARABOLIC BEHAVIOR FOR THE OXIDATION OF Co-25Cr AT LOW OXYGEN PRESSURES

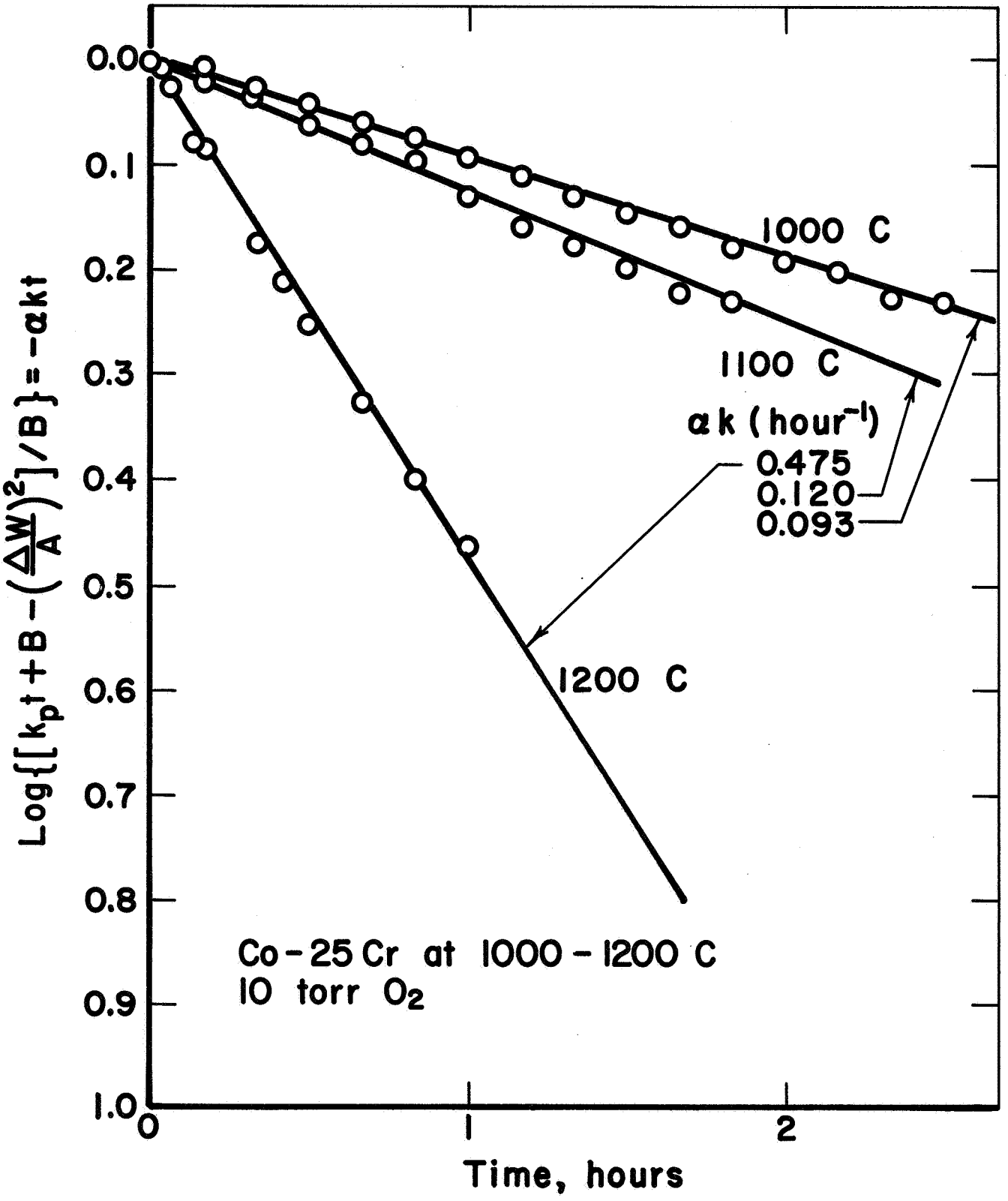

FIGURE 35. NORMALIZED DEVIATION FROM PARABOLIC BEHAVIOR FOR Co-25Cr ALLOYS OXIDIZED AT TEMPERATURES BETWEEN 1000 TO 1200 C AT LOW OXYGEN PRESSURES

REFERENCES

(1) Paidassi, J., Vallée, M. G., and Pepin, P., Mem. Sci. Rev. Met., 62, 789 (1965).

(2) Snide, J. A., Myers, J. R., and Saxer, R. K., Cobalt, 36, 157 (1967).

(3) "High-Temperature Oxidation of Alloys: Cobalt-Chromium Base Alloys", Kofstad, P., Hed, A. Z., Wilcox, B., and Clauer, A., NASA Research Grant NGR-36-002-070, First Semiannual Report (November 10, 1967).

PK/AZH:jbs/jls

DISTRIBUTION LIST

Grant NGR-36-002-070 – Battelle Memorial Institute
NASA Report No. CR-72420

	Copies
National Aeronautics and Space Administration Washington, D. C. 20546	
Attn: N. F. Rekos (RAP)	1
G. C. Deutsch (RRM)	1
R. H. Raring (RRM)	1
Winnie M. Morgan (US)	10
Lewis Research Center National Aeronautics and Space Administration 2100 Brookpark Road Cleveland, Ohio 44135	
Attn: G. M. Ault, MS-105-1	1
Technology Utilization, Office, MS-3-19	1
Dr. J. S. Wolf, MS-49-1	1
R. W. Hall, MS-105-1	1
Library, MS-60-3	2
Report Control Office, MS-5-5	1
S. J. Grisaffe, MS-49-1	1
Dr. H. B. Probst, MS-49-1	1
N. T. Saunders, MS-105-1	1
F. H. Harf, MS-106-1	5
A. E. Anglin, MS-106-1	1
C. E. Lowell, MS-49-1	1
J. C. Freche, MS-49-1	1
C. A. Barrett, MS-49-1	1
Langley Research Center National Aeronautics and Space Administration Langley Station Hampton, Virginia 23365	
Attn: Library	1
Richard Pride, MS-188A	1
George C. Marshall Space Flight Center National Aeronautics and Space Administration Marshall Space Flight Center, Alabama 35812	
Attn: Library	1
Jet Propulsion Laboratory 4800 Oak Grove Drive Pasadena, California 91103	
Attn: Library	1
Ames Research Center National Aeronautics and Space Administration Moffett Field, California 94035	
Attn: Library	1

	Copies
Goddard Space Flight Center National Aeronautics and Space Administration Greenbelt, Maryland 20771	
Attn: Library	1
D. F. Hasson, Code 714	1
C E. Vest, Code 249.1	1
Manned Spacecraft Center National Aeronautics and Space Administration Houston, Texas 77058	
Attn: Library	1
N. Chaffee, EB-4	1
Flight Research Center National Aeronautics and Space Administration P. O. Box 273 Edwards, California 93523	
Attn: Library	1
Federal Aviation Agency 800 Independence Avenue, SW Washington, D. C. 20553	
Attn: Brig. Gen. J. C. Maxwell	1
F. B. Howard, SS/210	1
Atomic Energy Commission Washington, D. C. 20545	
Attn: Technical Reports Library	1
Jules Simmons	1
Department of Air Force Office of Scientific Research Propulsion Research Division Washington, D. C. 20525	1
Headquarters Wright Patterson AFB, Ohio 45433	
Attn: MAAM: Technical Library	1
AFSC-FTDS	1
AFML: Dr. A. M. Lovelace	1
SESOS: J. L. Wilkins	1
MAMP: I. Perlmutter	1
Department of the Navy Office of Naval Research Code 429 Washington, D. C. 20525	
Attn: Dr. R. Roberts	1

DISTRIBUTION LIST (Continued)

	Copies
Chief, Bureau of Naval Weapons Department of the Navy Washington, D. C. 20525 Attn: T. F. Kearns	1
U. S. Army Aviation Materials Laboratory Fort Eustis, Virginia 23604 Attn: John White, Chief, SMOFE-APG	1
Army Materials Research Agency Watertown Arsenal Watertown, Massachusetts 02172 Attn: S. V. Arnold, Director	1
American Society for Metals Metals Park Novelty, Ohio 44073 Attn: Dr. Taylor Lyman	1
Defense Metals Information Center (DMIC) (1) Battelle Memorial Institute 505 King Avenue Columbus, Ohio 43201	1
The Bendix Corporation Research Laboratories Division Southfield, Michigan 48075 Attn: C. B. Sung	1
Boeing Company P. O. Box 733 Renton, Washington 98055 Attn: W. E. Binz, SST Unit Chief	1
General Electric Company Advanced Technology Laboratory Schenectady, New York 12305 Attn: Library	1
General Electric Company Materials Development Laboratory Operation Advance Engine and Tech. Department Cincinnati, Ohio 45215 Attn: L. P. Jahnke	1
General Motors Corporation Allison Division Indianapolis, Indiana 46206 Attn: D. K. Hanink, Materials Laboratory	1
International Nickel Company 67 Wall Street New York, New York 10005 Attn: R. R. Dewitt	1
International Nickel Company P. D Merica Research Laboratory Sterling Forest Suffern, New York 10901 Attn: Dr. F. Decker	1
Lockheed Palo Alto Research Laboratories Materials and Science Laboratory 52-30 3251 Hanover Street Palo Alto, California 94304 Attn: E. C. Burke	1
Narmco Research and Development Division Whittacker Corporation 3540 Aero Court San Diego, California 92123 Attn: Dr. F. J. Riel, Technical Director	1
Ohio State University Columbus, Ohio 43210 Attn: Professor M. G Fontana, Chairman Department of Metallurgical Engineering	1
Solar Division International Harvester Corporation San Diego, California 92112 Attn: J. V. Long, Director of Research	1
Stanford University Palo Alto, California 94305 Attn: Prof. Oleg Sherby Department of Materials Science	1
United Aircraft Corporation 400 Main Street East Hartford, Connecticut 06108 Attn: E. F. Bradley, Chief Materials Engineering	1

DISTRIBUTION LIST (Continued)

	Copies
University of California Los Angeles, California 90024 Attn: Dr. G. Hoffman	1
Tem-Pres Research, Inc. 1401 South Atherton Street State College, Pennsylvania 16801	1
Stanford Research Institute Menlo Park, California 94025 Attn: Dr. D. L. Douglass	1
General Electric Company Materials Development Laboratory Operation Advance Engine and Tech. Department Cincinnati, Ohio 45215 Attn: C. S. Wukusick	1
Ohio State University Columbus, Ohio 43210 Attn: Dr. A. R. Rapp Department of Metallurgical Engineering	1